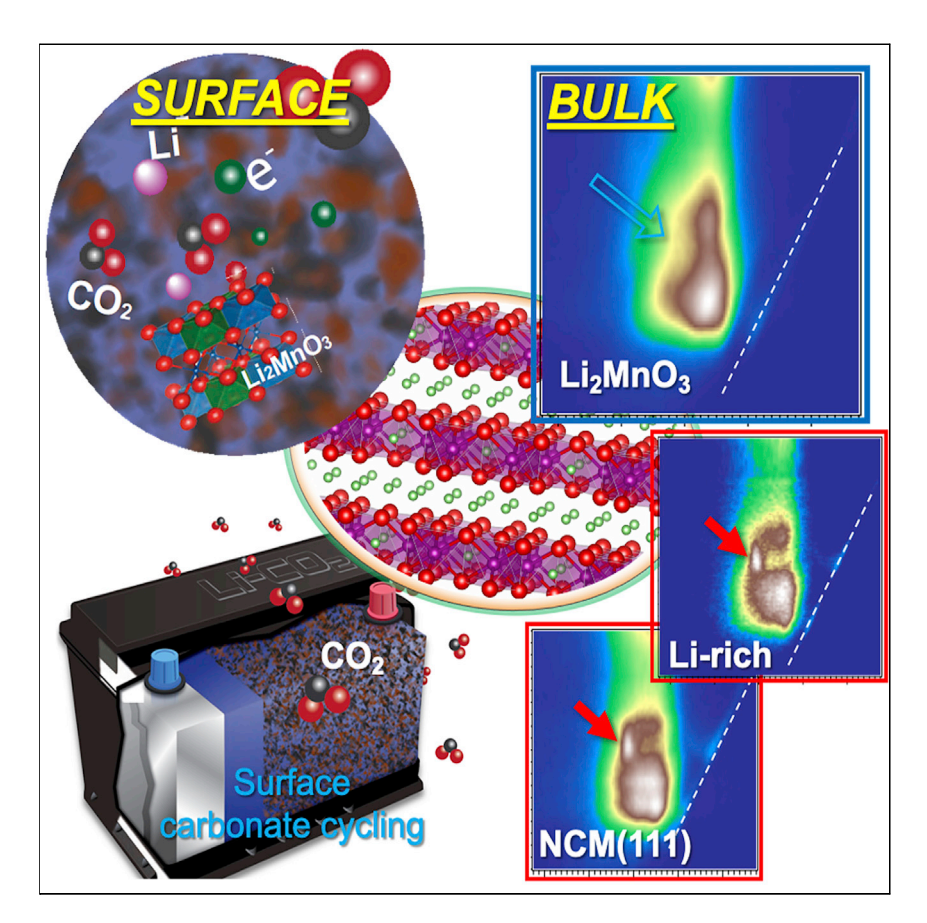
**Joule** 



### **Article**

# Cycling mechanism of Li<sub>2</sub>MnO<sub>3</sub>: Li– CO<sub>2</sub> batteries and commonality on oxygen redox in cathode materials



Li $_2$ MnO $_3$  is a parent compound of Li-rich materials whose electrochemical activities are under debate. Mn and O redox reactions are analyzed both in the bulk and on the surface during the initial and later cycles. Mn(III/IV) redox dominates the bulk reversible reactions in Li $_2$ MnO $_3$  with no lattice oxygen redox involved. The initial charge plateau is from various surface activities. Oxygen redox observed in Li-rich materials displays commonality in spectroscopic features compared with conventional materials. The highly reactive Li $_2$ MnO $_3$  surface enables an efficient catalytic reaction in Li-CO $_2$ /air batteries.

Zengqing Zhuo, Kehua Dai, Ruimin Qiao, ..., Hong Li, Thomas P. Devereaux, Wanli Yang

panfeng@pkusz.edu.cn (F.P.) hli@iphy.ac.cn (H.L.) tpd@stanford.edu (T.P.D.) wlyang@lbl.gov (W.Y.)

#### **HIGHLIGHTS**

Charge plateau of  $Li_2MnO_3$  is from oxygen release and surface carbonate reactions

Mn(III/IV) redox is solely responsible for the reversible bulk  ${\rm Li}_2{\rm MnO}_3$  cycling

Oxygen redox shares common nature in both Li-rich and conventional cathodes

Li<sub>2</sub>MnO<sub>3</sub> and alkali-rich materials could be superior catalysts for Li– CO<sub>2</sub>/air batteries

Zhuo et al., Joule 5, 975–997 April 21, 2021 © 2021 Elsevier Inc. https://doi.org/10.1016/j.joule.2021.02.004



**Joule** 



#### Article

## Cycling mechanism of Li<sub>2</sub>MnO<sub>3</sub>: Li–CO<sub>2</sub> batteries and commonality on oxygen redox in cathode materials

Zengging Zhuo, 1,2,11 Kehua Dai, 1,3,4,5,11 Ruimin Qiao, 1,11 Rui Wang, 6,11 Jinpeng Wu, 1,7,8 Yali Liu, 6 Jiayue Peng,<sup>6</sup> Liquan Chen,<sup>6</sup> Yi-de Chuang,<sup>1</sup> Feng Pan,<sup>2,\*</sup> Zhi-xun Shen,<sup>7,8,9</sup> Gao Liu,<sup>3</sup> Hong Li,<sup>6,\*</sup> Thomas P. Devereaux, 7,8,10,\* and Wanli Yang 1,12,\*

#### **SUMMARY**

Li<sub>2</sub>MnO<sub>3</sub> has been considered to be a representative Li-rich compound with active debates on oxygen activities. Here, by evaluating the Mn and O states in the bulk and on the surface of Li<sub>2</sub>MnO<sub>3</sub>, we clarify that Mn(III/IV) redox dominates the reversible bulk redox in Li<sub>2</sub>MnO<sub>3</sub>, while the initial charge plateau is from surface reactions with oxygen release and carbonate decomposition. No lattice oxygen redox is involved at any electrochemical stage. The carbonate formation and decomposition indicate the catalytic property of the Li<sub>2</sub>MnO<sub>3</sub> surface, which inspires Li-CO<sub>2</sub>/air batteries with Li<sub>2</sub>MnO<sub>3</sub> acting as a superior electrocatalyst. The absence of lattice oxygen redox in Li<sub>2</sub>MnO<sub>3</sub> questions the origin of the oxygen redox in Li-rich compounds, which is found to be of the same nature as that in conventional materials based on spectroscopic comparisons. These findings provide guidelines on understanding and controlling oxygen activities toward high-energy cathodes and suggest opportunities on using alkali-rich materials for catalytic reactions.

#### INTRODUCTION

The pressing demand for high-energy batteries has triggered tremendous efforts in the development of transition-metal-oxide (TMO)-based Li-ion battery (LIB) cathode materials operated at high voltages. 1-4 The high-voltage operation triggers complex chemical reactions, with its concepts and mechanism under active debate. One of the key practical concerns of the TMO electrode into the high-capacity high-voltage region is the spontaneous involvement of oxygen activities. If the oxygen activities are reversible oxygen redox reactions, they could potentially contribute to charge compensation for the high capacity. 5 However, if the reactions are irreversible oxygen oxidation and electrolyte decomposition, they lead to detrimental effects with irreversible oxygen release and parasitic surface reactions.<sup>6</sup> At present, both the fundamental understanding and the practical control of the oxygen reactions in TMO remain formidable challenges. In LIB research, majority of the studies on oxygen redox activities have been focused on layered Li-rich material, <sup>2,7-10</sup> a compound with excessive Li occupying part of the TM sites in the TM-O layer, which is typically described as  $xLi_2MnO_3 \cdot (1-x)LiMO_2$  (M = Ni, Co, Mn, etc.), indicating the "Li-rich" parent compound of Li<sub>2</sub>MnO<sub>3</sub> and the conventional part of LiMO<sub>2</sub>. 11

At present, it has been realized that the superior capacity of most Li-rich layered electrodes is enabled by the reversible oxygen redox reactions, confirmed by many experimental and theoretical studies.<sup>8,9,12</sup> Quantitative values of 44% retention rate of the

#### Context & scale

In the debates on how to achieve high energy density battery cathodes, Li-rich compounds are often considered superior over conventional materials due to their high capacity associated with the oxygen redox reactions. Here, we clarify both the bulk and surface reaction mechanisms of Li<sub>2</sub>MnO<sub>3</sub> during the initial and later cycles. Our results reveal that the initial charge plateau is from two types of surface activities, followed by predominating Mn redox reactions with no sign of reversible lattice oxygen redox. The surface chemistry of Li<sub>2</sub>MnO<sub>3</sub> indicates a highly reactive surface to facilitate carbonate formation and decomposition, inspiring a Li-CO<sub>2</sub>/air battery with Li<sub>2</sub>MnO<sub>3</sub> as a superior electrocatalyst. The comparison between Li-rich, conventional, and Li<sub>2</sub>MnO<sub>3</sub> suggests that the oxygen redox in Li-rich and conventional materials is of the same nature and origin.







oxygen redox reaction after 500 cycles are identified in a typical Li-rich material, Li<sub>1 17-</sub> Ni<sub>0.21</sub>Co<sub>0.08</sub>Mn<sub>0.54</sub>O<sub>2</sub>. <sup>13</sup> This is impressive, especially considering oxygen activities are often associated with fast decays. As another Li-rich system, the rock-salt disordered Li-rich materials could display a majority of cationic redox through fluorination <sup>14</sup>; however, oxygen redox activities are triggered in most of these materials too at high voltages, and fluorination is hard to achieve in layered compounds. 15 We, therefore, note that the discussions on the Li-rich material in this work refer to the Li-rich layered compounds without fluorination. Although oxygen redox has also been a topic of some non-Li-rich conventional LIB electrodes, 16-19 as well as some Na-ion compounds, 13,20-22 the oxygen redox almost always exhibits fast decay once triggered in conventional materials at high voltages, e.g., 63% of reversible oxygen redox is retained after only 10 cycles in the LiNi<sub>1/3</sub>Co<sub>1/3</sub>Mn<sub>1/3</sub>O<sub>2</sub> (NCM111) electrode. <sup>19</sup> Therefore, in LIB cathode research, Li-rich has been the role model of reversible oxygen redox and has dominated recent oxygen redox studies on both fundamental understandings and practical developments. 2,7-10,12,23-30

To clarify the discussions on the lattice oxygen reactions in this work, we should first try to define the scope of the oxygen redox concept. Unfortunately, the definition of the oxygen redox reaction has yet to be clearly established, mainly due to the elusive mechanism of the oxidized oxygen state that remains a challenging topic and is still under active debates. However, we could at least remove part of the common confusions by labeling what should not be considered as the oxidized oxygen states in the scope of oxygen redox concept: (1) the loss of electron density around an O atom through covalency or hybridization should not be considered as the oxidized oxygen in the oxygen redox concept, e.g., TM-O hybridized states or highly covalent states in molecules like CO<sub>2</sub>.<sup>31</sup> As a matter of fact, all TM-based battery cathodes display TM-O hybridization features in oxygen absorption spectroscopy, e.g., LiFePO<sub>4</sub>, and the hybridization gets enhanced upon electrochemical charging.<sup>32</sup> Therefore, depopulation of electrons around O through TM-O hybridization itself is not an oxidized oxygen state in oxygen redox concept, otherwise, all the TM-based cathode compounds, including LiFePO<sub>4</sub>, would be called oxygen redox systems. (2) A justified oxygen redox reaction should have at least one reversible cycle of oxidation ("ox") and reduction ("red") reactions. The obviously irreversible oxygen oxidation, e.g., released oxygen, should not be defined as oxygen "redox" reactions. For the same reason, the oxygen release signal itself does not signify lattice oxygen redox reactions. This is particularly important for understanding this work here. As we will see later, although Li<sub>2</sub>MnO<sub>3</sub> is well known to display a significant amount of gas released during charging, it does not involve any oxygen "redox" reaction in the lattice even in the very first cycle. However, it is important to emphasize that the regulations here do not mean the TM-O hybridization and oxygen release are unrelated to the lattice oxygen redox reactions; instead, they both show strong correlations with the oxygen redox behaviors on various properties, especially reversibility and stability, but with an unclear mechanism by this time.<sup>33</sup> Therefore, although the mechanism of the oxidized oxygen is still under debate, we could loosely define the lattice oxygen redox reaction in TMO-based battery cathodes: the oxygen oxidization in the oxygen redox concept should be a depopulation of oxygen electrons not through the TM-O hybridization itself but through a literal electron loss process such as a chemical peroxo-bond formation or a physical electron charge transfer from oxygen through a reshuffling of the electron states. Additionally, the reduction of the oxidized oxygen should take place for at least one cycle, otherwise, it is merely an irreversible oxygen oxidation process, which was found to take place mostly in the near-surface region.<sup>34</sup>

<sup>1</sup>Advanced Light Source, Lawrence Berkeley National Laboratory, Berkeley, CA 94720, USA

<sup>2</sup>School of Advanced Materials, Peking University Shenzhen Graduate School, Shenzhen 518055, China

<sup>3</sup>Energy Storage and Distributed Resources Division, Energy Technologies Area, Lawrence Berkeley National Laboratory, Berkeley, CA

<sup>4</sup>College of Chemistry, Tianjin Normal University, Tianjin 300387, China

<sup>5</sup>School of Metallurgy, Northeastern University, Shenyang 110819, China

<sup>6</sup>Institute of Physics, Chinese Academy of Sciences, Beijing 100190, China

<sup>7</sup>Stanford Institute for Materials and Energy Sciences, SLAC National Accelerator Laboratory, Menlo Park, CA 94025, USA

8Geballe Laboratory for Advanced Materials, Stanford University, Stanford, CA 94305, USA

<sup>9</sup>Department of Physics and Applied Physics, Stanford University, Stanford, CA 94305, USA

<sup>10</sup>Department of Materials Science and Engineering, Stanford University, Stanford, CA 94305, USA

<sup>11</sup>These authors contributed equally

<sup>12</sup>Lead contact

\*Correspondence: panfeng@pkusz.edu.cn (F.P.), hli@iphy.ac.cn (H.L.), tpd@stanford.edu (T.P.D.), wlyang@lbl.gov (W.Y.)

https://doi.org/10.1016/j.joule.2021.02.004





Electrochemically, Li<sub>2</sub>MnO<sub>3</sub> has long been identified to be responsible for the characteristic high-voltage plateau of Li-rich electrodes.<sup>35</sup> This plateau is now considered the region of oxygen oxidation reactions during the initial charge of Li-rich electrodes.  $^{2,9,12,13}$  As a result,  $Li_2MnO_3$  is often considered the key model system of a Li-rich configuration, which is defined in this work as a system with a considerable amount of lithium ions occupying the transition metal layer. Such a configuration has been widely believed to be responsible for the reversible oxygen redox reactions in Li-rich electrodes. <sup>23–27,36–38</sup> However, it is important to note that oxygen redox itself is not bound to this charging plateau, as evidenced by the clear signature of oxygen redox reactions in the Li-rich electrode over hundreds of extended cycles with a complete disappearance of the high-voltage plateau. 12 Therefore, the high-voltage plateau itself is not a fingerprint of the reversible oxygen redox and one should not attribute this initial charging of Li<sub>2</sub>MnO<sub>3</sub> to oxygen redox reactions merely because of its charging plateau.<sup>39</sup>

The reaction mechanism of Li<sub>2</sub>MnO<sub>3</sub> has seen a long history of contradictory debates between models of oxygen and Mn activities. Besides the early proposals of Mn<sup>4+/5+</sup> redox, <sup>40</sup> Li<sup>+</sup>/H<sup>+</sup> exchange, <sup>41</sup> and Li<sub>2</sub>O extraction, <sup>35</sup> etc., debates continue with revitalized concepts of reversible oxygen redox models, <sup>26,27</sup> irreversible oxygen release and surface reactions  $^{23-25,37,38,42,43}$ , and  $^{4+/7+}$  reactions  $^{36}$  Attributing the Li<sub>2</sub>MnO<sub>3</sub> cycling mechanism to reversible oxygen redox is mostly based on O-K Xray absorption spectroscopy (XAS) and photoelectron spectroscopy (XPS) results. 26,27 This model has been appreciated because it provides the natural rationality of the reversible oxygen redox found in Li-rich systems. However, recent clarifications have shown that XPS signals, even with hard X-rays, may not indicate the bulk oxygen states, 42 and variations of O-K XAS pre-edge is dominated by the changing TM characters and, thus, is not a reliable oxygen redox probe. 32,33 Other than the reversible oxygen redox model, it has long been known that the high-voltage plateau of Li<sub>2</sub>MnO<sub>3</sub> always comes with strong signals of oxygen release.<sup>38</sup> Theoretical works from Doublet et al. suggested the irreversible nature of the oxygen activities in Li<sub>2</sub>MnO<sub>3</sub>.<sup>24,25</sup> This is evaluated by Piper et al. through quantitative evaluations of the gas released during the initial cycle of Li<sub>2</sub>MnO<sub>3</sub>, suggesting a large part of the initial charging is from the irreversible oxygen oxidation,<sup>37</sup> followed by another consistent report.<sup>43</sup> However, these studies show that the oxygen release could compensate only part of the charge plateau. 37,38,43,44 Other than the arqument between the reversible and irreversible oxygen activities, Mn redox mechanism was re-proposed recently by Van der Ven et al., strongly concluding the Mn<sup>4+/7+</sup> redox reaction as the Li<sub>2</sub>MnO<sub>3</sub> charging mechanism through migrations into tetrahedral sites, which denies the involvements of oxygen oxidation.<sup>36</sup> However, in situ hard X-ray spectroscopic studies, as well as other experiments on magnetic property tests, found no evidence of such high valence Mn states. 45,46 Careful assessments also show that the oxidized oxygen signals found in spectroscopy are intrinsic and not from irradiation effects.<sup>47</sup> Therefore, despite the intensive efforts, critical questions remain on the Li<sub>2</sub>MnO<sub>3</sub> cycling mechanism, which is directly related to the "Li-rich" properties regarding oxygen activities. First, on the controversial reports of the reversible oxygen redox model, 26,27 versus the irreversible oxygen release model, 37,43 because the oxygen release cannot compensate all the charging plateau capacity, <sup>37,38,43,44</sup> is it possible that a finite amount of lattice oxygen redox is mixed with oxygen release at certain electrochemical stages, as often observed in other Li-rich systems?<sup>2,9,12,29,48</sup> Answering this question requires measurements of the chemical states at all critical electrochemical potentials. Second, if reversible oxygen redox reaction is not involved in Li<sub>2</sub>MnO<sub>3</sub> cycling, where does the extra capacity of the charge plateau come from other than the partial contribution from





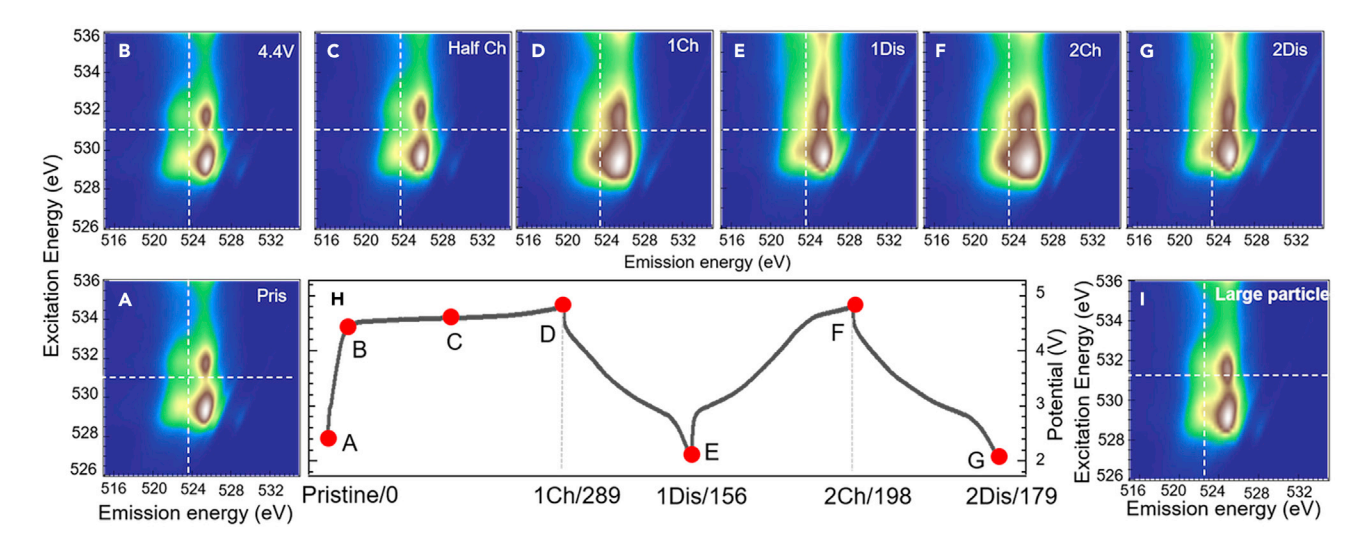


Figure 1. O-K mRIXS of a series of Li<sub>2</sub>MnO<sub>3</sub> electrodes at different electrochemical states

(A–G) mRIXS images collected from the electrodes with different state of charge indicated by the red dots on the electrochemical cycling profile in (H). Numbers following the charge (Ch) or discharge (Dis) notes are the corresponding capacity in each step with the unit of mAh g<sup>-1</sup>. Materials were synthesized with 450°C calcination temperature with a mean particle size of 70 nm. The crossing point of the white dashed lines indicate the typical position of expected sharp features of oxidized oxygen found in many Li-rich materials if lattice oxygen redox reactions were involved in the cycling. Horizontal dashed lines also indicate the excitation energy that one would expect enhanced low-energy-loss features close to the elastic line (rightmost faded line feature), which are not observed here either.

(I) is the mRIXS result collected from the electrode at 4.8 V charged state with material calcinated at 900°C with a mean particle size of about 140 nm.

oxygen release?  $^{37,38,43,44}$  Third, if  $\text{Li}_2\text{MnO}_3$  cycling does not involve reversible oxygen redox reactions, where does the capacity of the following discharge or the reversible cycling of  $\text{Li}_2\text{MnO}_3$  come from? Fourth, is  $\text{Mn}^{4+/7+}$  redox reaction responsible for the  $\text{Li}_2\text{MnO}_3$  cycling,  $^{36}$  especially if no reversible oxygen redox is found? Fifth, more importantly, with the clarified oxygen activities of  $\text{Li}_2\text{MnO}_3$ , does  $\text{Li}_2\text{MnO}_3$  provide the foundation for understanding the reversible oxygen redox activities in Li-rich layered compounds?

In order to answer all these questions, an unambiguous clarification of the reaction mechanism of both the O and Mn in the bulk and on the surface of  $\text{Li}_2\text{MnO}_3$  becomes necessary. Here, we carefully study and analyze the bulk and surface chemistry of the  $\text{Li}_2\text{MnO}_3$  materials prepared under different synthesis conditions, which lead to different particle sizes and surface area. In addition to the typical structural (Figures S1–S3) and electrochemical measurements (Figures S4 and S5), independent characterizations of both the Mn and O states of  $\text{Li}_2\text{MnO}_3$  at representative charge and discharge states are provided through state-of-the-art spectroscopic experiments with both surface and bulk sensitivities.

For the bulk cycling mechanism, we aim for direct answers to all the aforementioned questions based on evaluations of Mn and O states through high-efficiency mapping of resonant inelastic X-ray scattering (mRIXS), <sup>29</sup> which has been established as a tool-of-choice for quantifying the bulk Mn redox and for detecting the reversible oxygen redox reactions. <sup>2,12,13,16–19,48</sup> The probe depth of RIXS experiments is around 100–200 nm, which is comparable with the particle sizes here, as specified below. The bulk sensitivity of the RIXS analysis also benefits from the sharp contrasts of the signals from the surface and the bulk along with specific emission energies. <sup>12,13,39</sup> Our results of Mn and O consistently show that reversible oxygen redox reaction is not involved in any stage of the Li<sub>2</sub>MnO<sub>3</sub> cycling (Figure 1). Strikingly, the quantified



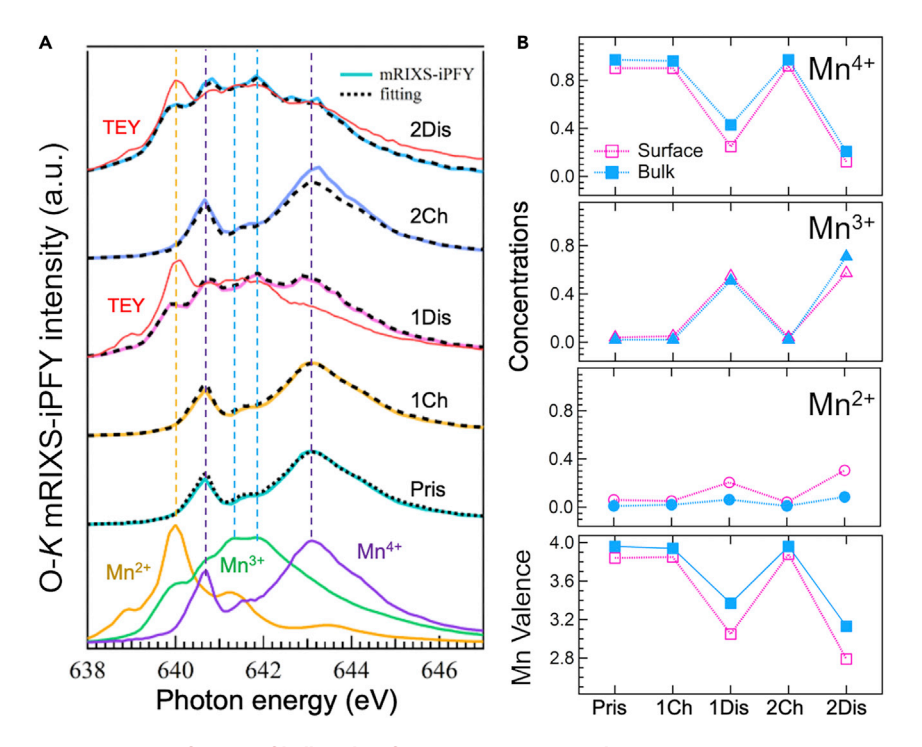


Figure 2. Quantification of bulk and surface Mn states upon cycling

(A) Mn-L<sub>3</sub> mRIXS-iPFY spectra (solid lines) with over-plotted fitting results (dashed lines). Two TEY spectra of the 1Dis and 2Dis are plotted here (red thin lines) to show the contrast between the surface and bulk Mn states. Raw mRIXS data and TEY spectra with fittings are presented in Figures S8 and S9, respectively. The excellent fitting is achieved by a simple linear combination of Mn<sup>2+</sup>/ Mn<sup>3+</sup>/Mn<sup>4+</sup> references as plotted at the bottom.

(B) shows the quantification results of the Mn valence contents, both in the bulk (through mRIXSiPFY fittings) and on the surface (through TEY fittings). Quantitative values are provided in Tables S1 and S2. The bottom panel displays the final results of the averaged Mn valence evolution upon cycling.

Mn<sup>3+/4+</sup> redox reaction could compensate almost all the discharge capacity immediately after the initial charging. After the initial cycle, a small amount of irreversible oxygen oxidation takes place during the 2<sup>nd</sup> charging, but Mn<sup>3+/4+</sup> redox remains the dominating contributor to the reversible part of the Li<sub>2</sub>MnO<sub>3</sub> cycling (Figures 2 and 3).

Clarifying the Li<sub>2</sub>MnO<sub>3</sub> bulk cycling mechanism raises two more crucial questions: (1) the reaction mechanism during the initial charging plateau and (2) the origin of the reversible oxygen redox in Li-rich materials. To answer the first question, we performed a detailed study of the surface chemical evolution. In addition to the many previous works on oxygen release, 37,38 our surface data reveal a clear signature of surface carbonate cycling (Figures 4 and 5). The surface of Li<sub>2</sub>MnO<sub>3</sub> particles is highly reactive to the electrolyte even without electrochemical potential, indicating a strong catalytic nature. The decomposition of this pre-formed surface carbonate, combined with the oxygen release, is responsible for the charge plateau capacity (Figure 6). Furthermore, the intriguing finding of a relatively reversible surface carbonate cycling on large particles inspires a demonstration of a Li-CO<sub>2</sub> battery with Li<sub>2</sub>MnO<sub>3</sub> as an effective electrocatalyst, which displays a fairly reversible high capacity compared with the systems based on other typical TMO catalysts (Figure 7). To answer the second question, we performed a direct comparison of the oxygen mRIXS features in all the relevant compounds of charged Li-rich, NCM111, LiCoO<sub>2</sub>, LiNiO<sub>2</sub>, and Li<sub>2</sub>MnO<sub>3</sub> (Figure 8). The comparison shows that reversible oxygen redox





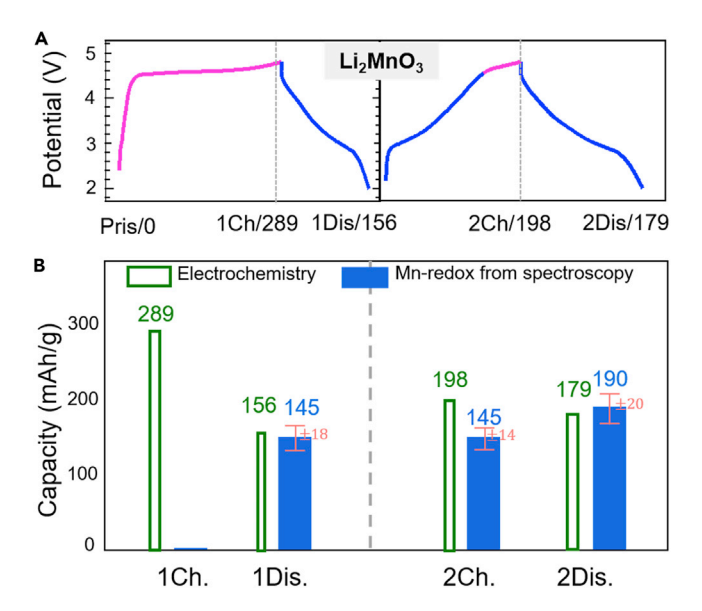


Figure 3. Cycling mechanism of Li<sub>2</sub>MnO<sub>3</sub>

(A) is the cycling profile with electrochemical capacity values of each charge (Ch) and discharge (Dis) step with a unit of mAh  $g^{-1}$ . Colors of the profile lines represent roughly the different redox mechanism, blue for reversible Mn<sup>3+/4+</sup> and pink for irreversible reactions invoving oxygen release and surface reactions.

(B) shows the quantified  $Mn^{3+/4+}$  redox reactions (blue) compared directly with electrochemical capacity. Mn redox fully covers the discharge capacity in both cycles, with irreversible reactions during the initial charging and part of the  $2^{nd}$  charging.

reaction in Li-rich resembles those in conventional materials, implying that oxygen redox is a common property of most TMO cathodes at highly oxidized states, and the Li-rich configuration only "affect" oxygen redox behavior, by either over-promoting irreversible oxygen oxidation in systems like  $\rm Li_2MnO_3$  or improving its reversibility in other systems like Li-rich.

#### **RESULTS AND DISCUSSION**

#### Material synthesis, structure, and electrochemistry

In order to confirm the robustness of the results, we have tested Li<sub>2</sub>MnO<sub>3</sub> materials with different particle sizes and surface areas, synthesized in different ways, with different precursors, and by different battery material groups. Technical details on material synthesis are provided in Supplemental information. In general, materials were prepared in two different ways by poly (vinyl pyrrolidone) (PVP)-assisted gel combustion method and solid-state reaction method with different calcination temperatures of 400°C, 450°C, 800°C, and 900°C. The structure and its evolution of the material synthesized through standard solid-state reaction have been reported previously in detail through X-ray diffraction (XRD), spherical aberration-corrected scanning transmission electron microscopy (STEM), and neutron diffraction.<sup>49</sup> We noticed the material prepared by PVP-assisted combustion method shows a better crystallization, which has been demonstrated in other battery cathode materials.<sup>50</sup> The better crystallization leads to a bit larger particle size in general, compared with the materials prepared by solid-state reactions. However, the materials prepared in different synthesis methods display the same trend of the particle size increase upon calcination temperature. More importantly, they display the same electrochemical profile variation upon calcination temperatures, as well as spectroscopic results, as described below, indicating the robustness of our findings among all Li<sub>2</sub>MnO<sub>3</sub> materials prepared through different synthesis methods and/or conditions.



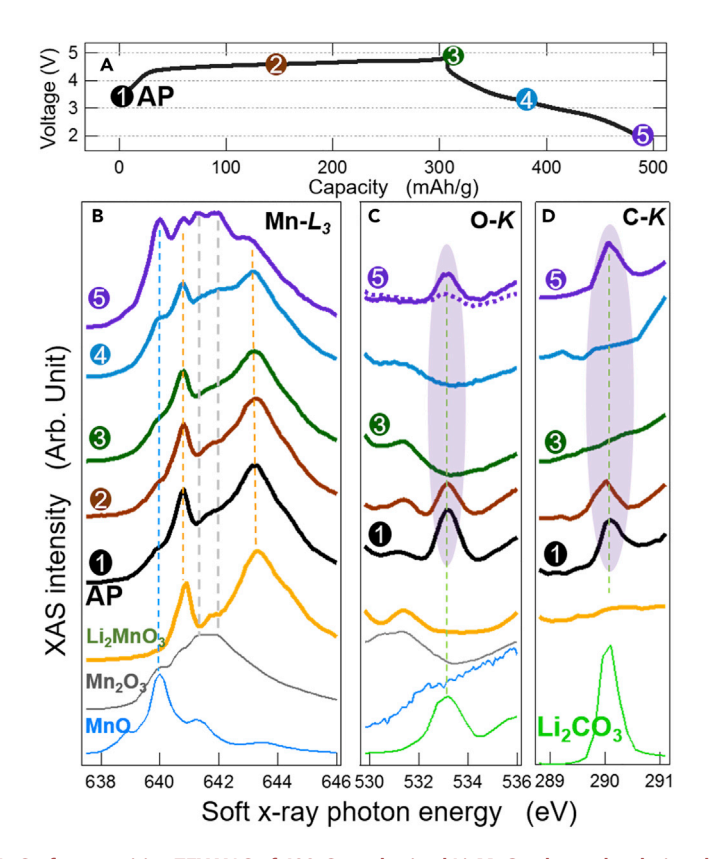


Figure 4. Surface-sensitive TEY XAS of  $400^{\circ}\text{C-synthesized Li}_2\text{MnO}_3$  electrodes during the first electrochemical cycle

(A) Electrochemical states of the samples marked on cycling curves.

(B–D) (B) Mn-L, (C) O-K, and (D) C-K XAS of reference samples (bottom) and cycled  $Li_2MnO_3$  electrodes. All spectra are collected in TEY mode, expect the dotted line of sample #5 in (C) that is the O-K TFY spectrum for comparison. Dashed lines and ovals indicate the major Mn and  $Li_2CO_3$  spectroscopic features. Full energy range TEY and TFY spectra over extended cycles are presented in Figures S10, S11, and S14. Only the Mn- $L_3$  and carbonate features are displayed in the main figure here. " $Li_2MnO_3$ " samples are pristine  $Li_2MnO_3$  powders. "AP" samples are as-prepared  $Li_2MnO_3$  electrodes that are exposed to electrolyte but before any electrochemical cycle. All electrode samples are carefully washed and handled as described in Supplemental experimental procedures.

As in previous reports, <sup>38,49</sup> the different Li<sub>2</sub>MnO<sub>3</sub> calcination temperatures lead to very different particle sizes, as well as different levels of crystallization. Figure S1 presents the SEM images of the 450°C and 900°C samples prepared by the PVP-assisted combustion method, with the mean particle sizes of 70 and 140 nm, respectively. Other than the large particle size, the material calcined at high temperature displays much sharper peaks in XRD patterns, indicating better crystallization than the low-temperature materials. Note again that the materials synthesized through the standard solid-state reaction display exactly the same trend in particle size and crystallization, which have been reported previously. 38,49 Figure S2 displays the XRD patterns and corresponding Rietveld refinements of the same 450°C and 900°C calcined materials. All peaks from both samples can be indexed to a typical monoclinic layer structure (ICDD PDF #04-011-3411) with C2/m space group. The XRD patterns are refined with the same Li<sub>2</sub>MnO<sub>3</sub> structure with C2/m space group, and the results along with refined cell parameters are shown in Figure S2. Relatively, Li<sub>2</sub>MnO<sub>3</sub> materials synthesized through standard solid-state reactions display less crystallization (Figure S3) with the detailed structural study of the same material in a previous report,  $^{49}$  again, consistent with previous reports on  $Li_2MnO_3$  materials

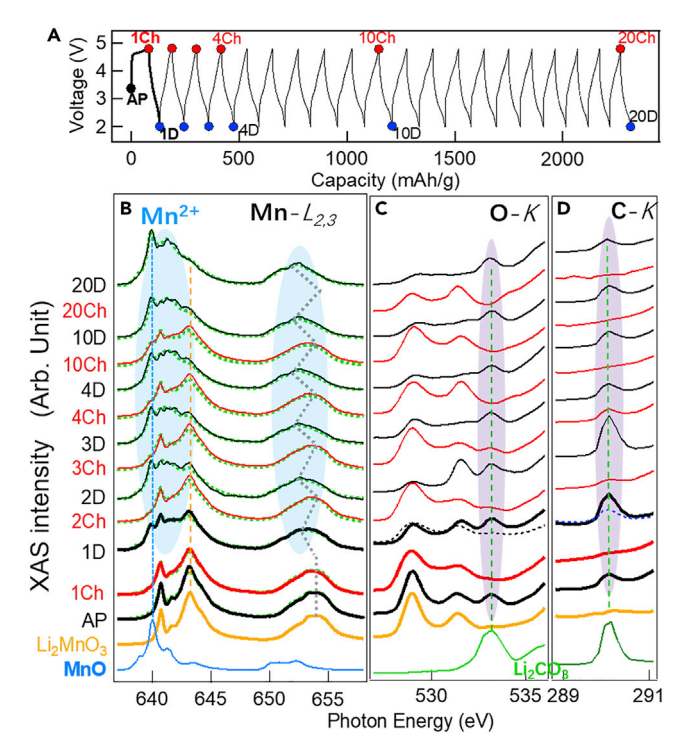


Figure 5. Surface-sensitive TEY XAS of cycled 800°C-synthesized Li<sub>2</sub>MnO<sub>3</sub> electrodes
(A) Electrochemical states of the samples.
(B–D) (B) Mn-L, (C) O-K, and (D) C-K XAS of the cycled Li<sub>2</sub>MnO<sub>3</sub> electrodes, as well as Mn<sup>2+</sup> and Li<sub>2</sub>CO<sub>3</sub> references (bottom). Dotted green lines in (B) are fittings to obtain Mn valence concentrations. Dotted black lines of "1D" in (C) and (D) are TFY spectra for comparison. Full energy range TEY and TFY spectra are presented in Figures S12, S13, and S15. The evolving carbonate and Mn peaks are emphasized by the shaded ovals and dashed lines.

from many groups. <sup>51–56</sup> Upon electrochemical cycling, the material crystallization is largely damaged and the detailed structural changes during the initial delithiation and relithiation process have been studied to reveal the amorphousness, disrupted Li/Mn ordering in the transition metal layer, and the development of the spinel phase in previous reports. <sup>38,49,51–57</sup>

The electrochemical profile of Li<sub>2</sub>MnO<sub>3</sub> has also been reported previously, <sup>38,49,54,56,57</sup> which has well documented that, compared with the high-temperature calcined materials, the low-temperature materials display a much higher capacity, especially on the charging plateau during the initial cycle. The high-temperature material displays a low capacity, however, with better capacity retention upon cycling. Figure S4 shows the charge and discharge profiles of Li<sub>2</sub>MnO<sub>3</sub> synthesized through solid-state reactions at 400°C and 800°C. All electrodes show the characteristic and irreversible 4.5 V plateau in the initial charge cycle, with higher capacity (270 mAh  $g^{-1}$ ) of 400°C samples than that of 800°C samples  $(82 \text{ mAh g}^{-1})$ . The high-temperature material displays better capacity retention, and the dQ/dV also displays a better sustained 4.5 V feature, mechanism of which will be clarified later in this work. Figure S5 displays the electrochemical profile of Li<sub>2</sub>MnO<sub>3</sub> synthesized by PVP-assisted combustion method at 450°C and 900°C, with capacities of 290 and 95 mAh g<sup>-1</sup> during the initial charging, respectively. Despite the quantitative differences of the materials synthesized by different methods, which should be related with the better crystallization of the PVP-assisted combustion method as mentioned above, all the electrochemical behaviors, e.g., capacity



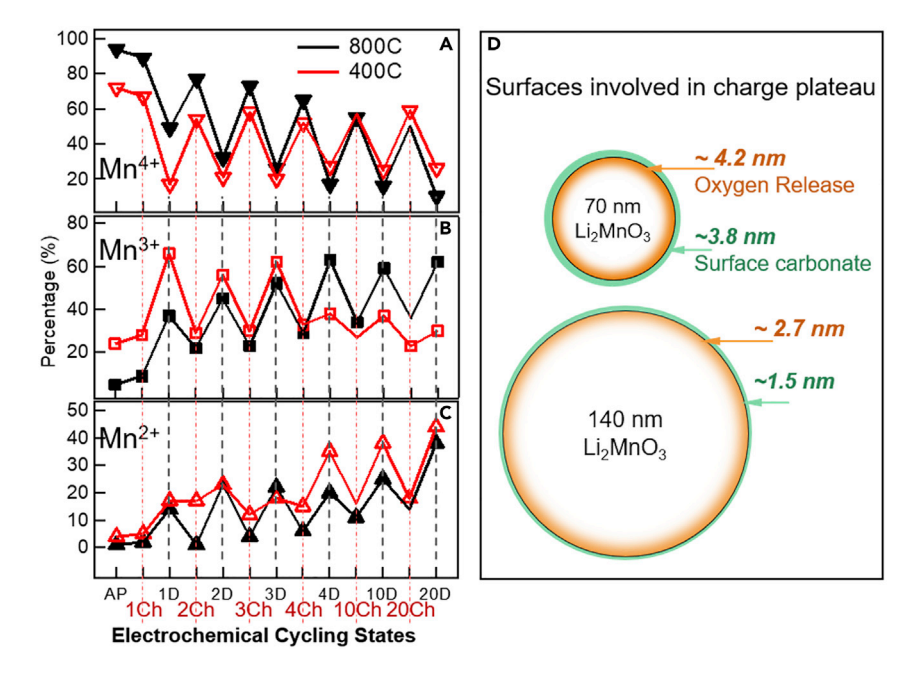


Figure 6. Quantified surface Mn oxidation states in Li<sub>2</sub>MnO<sub>3</sub> electrodes over extended cycles and schematics of the surface reaction layer thickness during the initial charge

(A-C) The concentration of (A) Mn<sup>4+</sup>, (B) Mn<sup>3+</sup>, and (C) Mn<sup>2+</sup> are obtained by fitting experimental Mn-L XAS data (dotted green lines in Figures 5B, S14, and S15) with a linear combination of the Mn reference spectra. Mn<sup>2+</sup> emerges from the 1st discharged state with the overall amount increasing upon cycling in both 400°C and 800°C-synthesized samples.

(D) Schematics of the two types of surface reactions that contribute to the initial charge plateau: the oxygen oxidation upon material delithiation in the form of oxygen release and the surface carbonate decomposition. Both reactions are within several nanometers of the particle surface, with a thicker active layer on smaller particles, as estimated in the section, "The origin of the highvoltage charge plateau of Li<sub>2</sub>MnO<sub>3</sub>.".

changes upon calcination temperatures, capacity retention, cycling lineshapes, etc., are typical properties of Li<sub>2</sub>MnO<sub>3</sub>, consistent with the previous studies.<sup>38,49,54,56,57</sup> Additionally, we note that, for the spectroscopic experiments, we have tested electrodes in charged states in different types of cells, i.e., coin, pouch, and Swagelok cells, but found no difference among the results.

#### Searching for lattice oxygen redox in Li<sub>2</sub>MnO<sub>3</sub>

Figure 1 displays the O-K mRIXS images of a series of Li<sub>2</sub>MnO<sub>3</sub> electrodes, based on materials calcined at 450°C, at different charge/discharge states indicated on the cycling curve. All the main mRIXS features are from Mn-O hybridization states, <sup>29,48</sup> which get broadened and strengthened in charged states (Figures 1D and 1F). Such a variation is consistent with the intensity increase in O-K XAS (Figure S6), but it is only from the enhanced Mn-O hybridization upon charging and is not a probe of oxidized oxygen. 32,33 As reported in previous reports of Li-rich electrodes, <sup>2,9,12,29,48</sup> mRIXS detects the latticed oxidized oxygen through two coexisting characteristic features in charged states: (1) a sharp feature around 531 and 524 eV excitation and emission energies, respectively, <sup>2,9,12,29,33,48</sup> and (2) a low-energy-loss feature close to the elastic line at the same excitation energy. 16,48 These features are generally consistent with the oxidized oxygen states in molecular systems of Li<sub>2</sub>O<sub>2</sub> and O<sub>2</sub>, but with certain spectroscopic contrasts.31,58 As indicated by the white dashed lines in Figure 1, none of these lattice oxidized oxygen features could be observed throughout the cycling of Li<sub>2</sub>MnO<sub>3</sub>. Furthermore, Figure 11 displays the mRIXS result of the charged electrode prepared with the





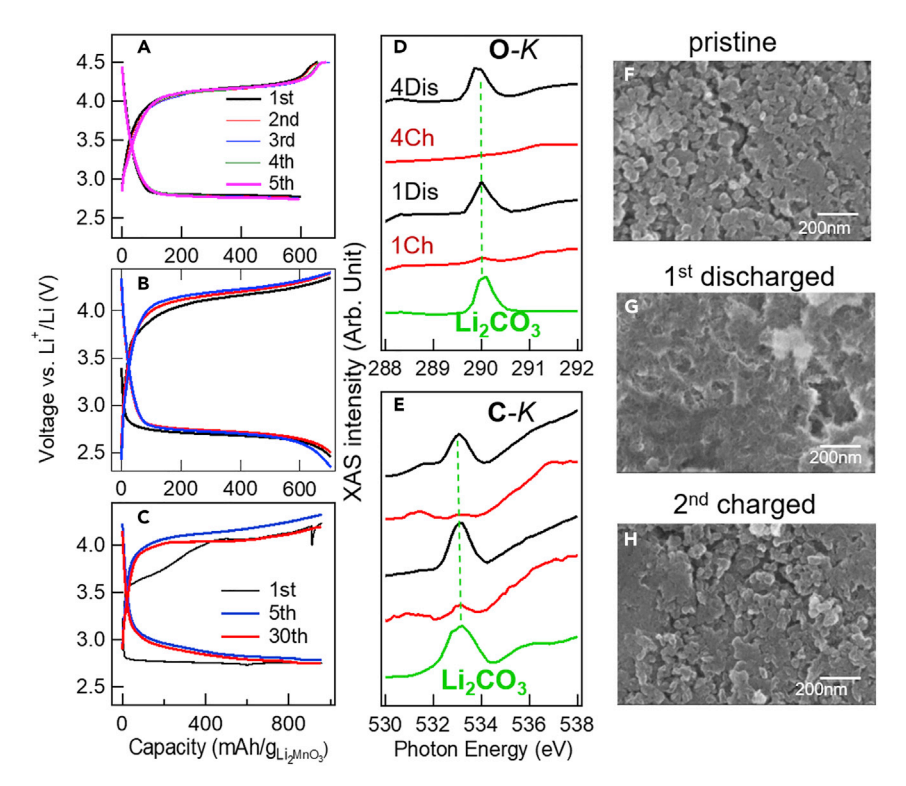


Figure 7. Li-CO<sub>2</sub>:O<sub>2</sub> (2:1) and Li-CO<sub>2</sub> batteries with Li<sub>2</sub>MnO<sub>3</sub> based electrocatalyst

(A) Electrochemical cycling of a Li-CO $_2$ :O $_2$  (2:1) cell with the EC/DMC electrolyte. (B) Electrochemical cycling of a Li-CO $_2$  cell with the same electrolyte. (C) Electrochemical cycling of a Li-CO $_2$ :O $_2$  (2:1) cell with LiCF $_3$ SO $_3$ /TEGDME (1:4) electrolyte. (D and E) (D) C-K and (E) O-K XAS TEY spectra of the Li $_2$ MnO $_3$  electrodes that are cycled to the 1st and 4th charged (Ch) and discharged (Dis) states. Carbonate cycling is indicated by its characteristic XAS peaks marked by dashed lines. Full energy range TEY and TFY data are shown in Figures S17 and S18.

(F–H) SEM images show the morphology change of  $Li_2MnO_3$  electrodes in  $Li-CO_2:O_2$  cells, including the pristine (F), 1st cycle discharged (G), and 2nd cycle charged (H) electrodes.

material calcinated at 900°C with a large (140 nm) mean particle size. Still, no oxidized oxygen feature could be observed. Note again that the missing signature of oxidized oxygen in Li<sub>2</sub>MnO<sub>3</sub> thin films and the 1<sup>st</sup> cycle fully charged state have been noticed before; <sup>28,37</sup> the thorough investigation here concludes that the lattice oxygen redox reaction never takes place at any electrochemical stage. A model of trapped O<sub>2</sub> molecule has been recently proposed as the oxidized oxygen state in Li-rich materials. <sup>21,36,59</sup> However, we have not observed any particle size effect here on the absence of oxidized oxygen species in Li<sub>2</sub>MnO<sub>3</sub> particles of 70 and 140 nm. More specific discussions on the trapped O<sub>2</sub> model are provided later in the discussions.

#### The reversible reaction of Li<sub>2</sub>MnO<sub>3</sub> cycling

A critical question emerges now on how  $\rm Li_2MnO_3$  could be electrochemically active with reversible charge/discharge capacities without lattice oxygen redox. Mn becomes the only candidate for reversible redox reactions. As reviewed above, the  $\rm Mn^{4+/7+}$  redox couple has been proposed very recently to explain the reversible cycling. However, even with *in situ* experiments, hard X-ray TM-K studies of Lirich compounds found only decreased TM oxidation states upon discharge. Technically, it is difficult to use Mn-K for quantitative analysis of Mn states, as both the edge position and the lineshape could vary significantly even with the same Mn



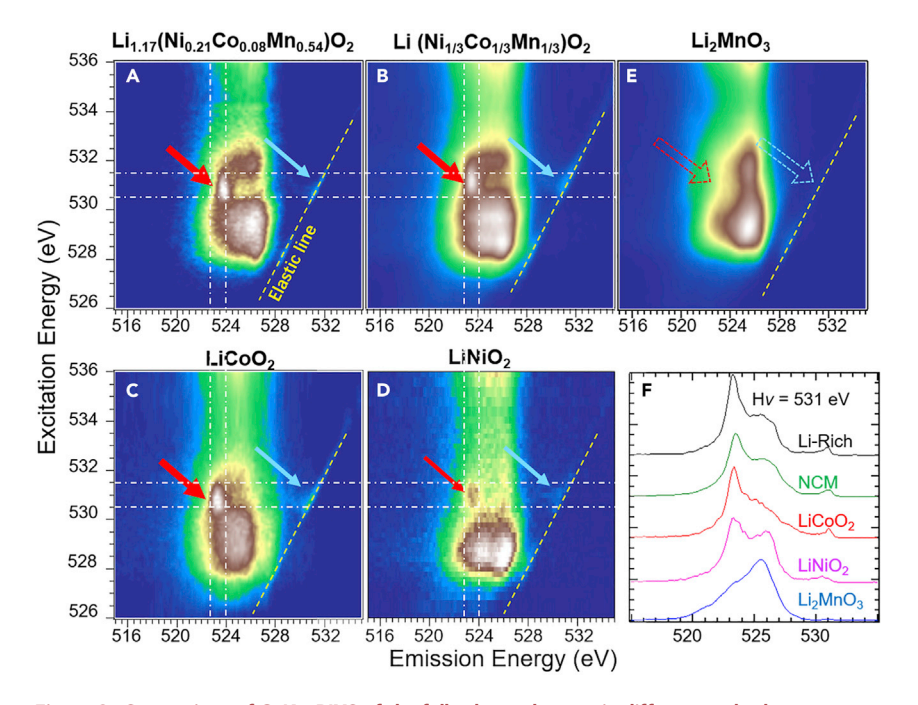


Figure 8. Comparison of O-K mRIXS of the fully charged states in different cathode systems (A-E) were collected from the 1st cycle fully charged electrodes of (A) Li<sub>1.17</sub>(Ni<sub>0.21</sub>Co<sub>0.08</sub>Mn<sub>0.54</sub>)O<sub>2</sub>, reproduced from Gent et al.  $^{12}$  with permission, (B) Li (Ni  $_{1/3}$  Co  $_{1/3}$  Mn  $_{1/3}$  )O  $_2$  , reproduced from Lee et al. <sup>19</sup> with permission, and (E)  $Li_2MnO_3$ , as well as remotely related (C)  $LiCoO_2$ , reproduced from Zhang et al.  $^{18}$  with permission, and (D) LiNiO<sub>2</sub>, reproduced from Li et al.  $^{17}$  with permission. mRIXS results of these electrodes at other electrochemical states, e.g., pristine or discharged, could be found in the previous reports as listed here. Horizontal and vertical dashed white lines are guides to eyes for direct position comparison. Diagonal yellow dashed lines indicate the elastic lines, i.e., the line with the same excitation and emission energies.

(F) is a lineshape comparison of the RIXS cuts at 531 eV excitation energy of all the electrodes.

valence. 61 Mn-L offers direct measurements of the 3d valence states that could be quantified to calculate the capacity contribution. 62 The only Mn-L edge study of Li<sub>2</sub>MnO<sub>3</sub> we could find is through conventional XAS, mainly showing the Mn<sup>2+</sup> developed on the surface.<sup>26</sup> As a matter of fact, it is known that the bulk-sensitive Mn-L through the fluorescence yield (FY) in conventional XAS technique suffers lineshape distortions that hinder the quantitative analysis (Figures S7B, S14, and S15).<sup>29</sup>

In order to provide a quantitative evaluation of the bulk Mn redox and compare it with the Li<sub>2</sub>MnO<sub>3</sub> capacity, we combined the quantitative fitting methods,<sup>62</sup> with the inverse partial FY (iPFY) signals extracted from Mn-L mRIXS experiments.<sup>29</sup> We note that such a quantitative evaluation of Mn redox reactions based on the fitting of mRIXS-iPFY has been demonstrated in many reports of Li-ion and Na-ion electrodes. 6,13,30 With the technical details provided in Supplemental information and Figures S7 and 2A presents the mRIXS-iPFY spectra (extracted from mRIXS images in Figure S8), over-plotted by their quantitative fittings (dotted lines) with excellent agreements. The fitting results of the Mn valence contents and averaged valence at different electrochemical states are provided in Table S1 and plotted in Figure 2B. In comparison, we also collected the surface-sensitive total electron yield (TEY) signals of Mn-L XAS and performed the same detailed fittings (Table S2; Figure S9). The strong contrast between the TEY surface and mRIXS-iFPY bulk signals, especially on the surface Mn<sup>2+</sup> (Figure 2), indicates the different surface/bulk reactions detected by the two techniques, and both could be quantified through the





demonstrated fitting method and are presented in Figure 2B. Below, we elaborate on the bulk redox behaviors first, then the surface activities.

The quantitative values of Mn oxidation states based on mRIXS-iPFY at different charge-discharge states define the electron charge transfer numbers through Mn redox reactions, providing directly the amount of Mn redox reactions in Li<sub>2</sub>MnO<sub>3</sub>. Figures 3A and 3B visualize the amount of Mn redox in direct comparison with the electrochemical capacity. Amazingly, the discharge capacity right after the initial charging could all be compensated by Mn<sup>3+/4+</sup> redox reactions. Mn<sup>3+/4+</sup> redox is responsible for the reversible cycling in the 2<sup>nd</sup> cycle too, but with a small amount of non-Mn<sup>3+/4+</sup> activity during the 2<sup>nd</sup> charging, which is again irreversible as evidenced by the pure Mn<sup>3+/4+</sup> redox during the 2<sup>nd</sup> discharge. The quantitative analysis of the Mn<sup>3+/4+</sup> reaction here not only reveals the origin of the reversible cycling of Li<sub>2</sub>MnO<sub>3</sub>, it also indicates no oxygen reduction reaction is involved during the discharge process, supporting directly the findings through O-K mRIXS on the absence of reversible oxygen redox reaction in Li<sub>2</sub>MnO<sub>3</sub>.

#### The highly reactive Li<sub>2</sub>MnO<sub>3</sub> surface and carbonate cycling

The aforementioned quantification of the bulk Mn redox contribution reveals the Mn-redox dominated reversible cycling of Li<sub>2</sub>MnO<sub>3</sub> right after the initial charging, indicating a different nature of the reactions during the initial charging. As a matter of fact, the initial charging mechanism of Li<sub>2</sub>MnO<sub>3</sub> has been the central topic of many studies. <sup>23–25,37,38,43</sup> The studies have indicated two important parts of the reaction mechanism during the initial charging, the oxygen release and the surface reactions. Gas release tests have been extensively performed on Li-rich materials, including Li<sub>2</sub>MnO<sub>3</sub>, since it was found to be electrochemically active.<sup>38</sup> A significant amount of  $O_2$  and  $CO_2$  gas release could be observed during the initial charging of  $Li_2MnO_3$ . A recent gas release and titration evaluation shows that the O<sub>2</sub> and CO<sub>2</sub> gas release could compensate for a large fraction of the charging capacity.<sup>37</sup> Furthermore, studies also suggest the CO<sub>2</sub> gas release is from the reaction of the evolved singlet <sup>1</sup>O<sub>2</sub> with the electrolyte on the electrode surface. <sup>43,63</sup> Still, all these gas release analyses have found that the initial charge capacity cannot be all compensated by the oxygen release, <sup>37,38,43,44</sup> i.e., other reaction mechanisms during the initial charging need to be clarified.

In addition to the gas release studies during the Li<sub>2</sub>MnO<sub>3</sub> initial charging, many works have implied the crucial role of surface reactions in Li<sub>2</sub>MnO<sub>3</sub> electrodes. For example, at temperatures above 50°C, Li-rich electrodes display anomalous capacity exceeding the theoretical value. 64,65 This high-temperature capacity gain was also observed in pure Li<sub>2</sub>MnO<sub>3</sub>, accompanied by significantly enhanced CO<sub>2</sub> gas release.<sup>38</sup> The involvement of carbon species implies the importance of surface reactions with the electrolyte. Additionally, the capacity of the initial charge plateau also depends on the synthesis temperature of Li<sub>2</sub>MnO<sub>3</sub> materials. As discussed above, a lower synthesis temperature leads to smaller particle size, thus larger surface area, which increases the initial charging capacity (Figures S1 and S3-S5). Particularly, Yu et al. have shown a positive linear relationship between the capacity and specific surface area of Li<sub>2</sub>MnO<sub>3</sub>, <sup>38</sup> directly suggesting again the significant role of surface activities during the Li<sub>2</sub>MnO<sub>3</sub> initial charging. Therefore, we perform a detailed and systematic study of the Li<sub>2</sub>MnO<sub>3</sub> surface chemistry at different electrochemical states over extended cycles through both the surface-sensitive (about 10 nm probe depth) TEY and bulk-sensitive (100–200 nm probe depth) total fluorescence yield (TFY) channels of soft X-ray XAS experiments in all the elemental edges, i.e., Li-K, Mn-L, O-K, and C-K (Figures S10-S16).





Figure 4 displays the XAS TEY spectra collected from a series of electrodes based on the 400°C calcined materials at different electrochemical potentials. The surface Mn state evolves in the same way as that of the 450°C samples discussed above (Figures 2 and S9; Table S2), with surface Mn<sup>2+</sup> species clearly observed after the initial cycle. All the Mn-L spectra are quantitatively fitted and will be discussed further below with the 800°C calcined samples. Here, we focus on the surface signals from O-K and C-K. The full range of TEY and TFY spectra are shown in Figures \$10 and \$11. Figures 4C and 4D zoom in on the evolving features that are aligned with the Li<sub>2</sub>CO<sub>3</sub> fingerprinting signals. A small amount of carbonate signal in the assynthesized Li<sub>2</sub>MnO<sub>3</sub> could be seen from the TFY spectra (Figure S10), indicating a typical carbonate impurity specie from sample synthesis. Strikingly, the as-prepared (marked as "AP") electrode before any electrochemical cycling, but with exposure to the electrolyte (then washed with dimethyl carbonate (DMC), see Supplemental experimental procedures), displays clear signatures of carbonate species, especially in the surface-sensitive TEY signals. This is in contrast with the carbonate impurity signal that is weak and relatively stronger in the bulk-sensitive TFY signals (Figure S10). The strong carbonate signal of the AP electrode suggests that carbonates are formed on the surface of pristine Li<sub>2</sub>MnO<sub>3</sub> particles before any electrochemical cycling, i.e., this initial carbonate formation does not rely on the oxygen evolution from Li<sub>2</sub>MnO<sub>3</sub>, instead, it indicates a highly reactive Li<sub>2</sub>MnO<sub>3</sub> surface when contacting the electrolyte.

The carbonate signal disappears upon charging, then reappears after the first-cycle discharge. But it does not show up again after the  $2^{nd}$  cycle charging (Figure S10). So the surface carbonate seems to be reversibly formed and decomposed for only one cycle on the  $400^{\circ}$ C-synthesized particles.

Figure 5 displays the evolving features in XAS TEY spectra of the electrode based on 800 °C calcined materials, with the full O-K and C-K TEY and TFY spectra in Figures S12 and S13. Due to the higher calcination temperature, the material impurity of the carbonate species is negligible even in the TFY spectrum (Figure S12). The same surface reaction takes place and a clear peak of carbonate appears with the as-prepared electrode (AP) after the exposure to electrolyte before cycling. For the 400°C samples, the surface carbonate becomes negligible after the 2<sup>nd</sup> cycle charge. However, for the 800°C samples, the appearance and disappearance of the carbonate signals in both O-K and C-K during discharging and charging could be clearly seen even after 20 cycles, indicating a relatively more reversible surface carbonate formation and decomposition over extended cycles.

In addition to the carbonate signals, we have quantitatively fitted all the surface-sensitive Mn-L TEY spectra collected from the 400°C and 800°C samples (Figures 5A, S14, and S15) based on a linear combination of the Mn reference spectra. Excellent fittings have been achieved (dashed lines in the figures), and the results are displayed in Figure 6, showing a consistent surface Mn behavior upon cycling over extended cycles. Upon cycling, surface Mn<sup>2+</sup> increases from around 5% to 40% from the 1<sup>st</sup> discharged (1D) to the 20<sup>th</sup> discharged (20D) states. The Mn<sup>2+</sup> specie accumulates on the surface, so even in the charged states, there is a significant amount of Mn<sup>2+</sup> after extended cycles, which could also be seen directly through the 640 eV peaks in Mn-L spectra (Figures 5A, S14, and S15). We note again that this surface behavior is the same as that of the 450°C samples prepared differently (Figure 2). Furthermore, the zig-zag patterns of the Mn-L<sub>2</sub> feature, although cannot be used for quantitative evaluation, could be seen in bulk-sensitive TFY results too (Figures S14 and S15), which indicate the reversible bulk Mn redox chemistry over





extended cycles, again consistent with the quantified results from the 450°C samples based on mRIXS-iPFY analysis (Figures 2, 3, and S8).

#### The origin of the high-voltage charge plateau of Li<sub>2</sub>MnO<sub>3</sub>

The study of the surface activities of Li<sub>2</sub>MnO<sub>3</sub> materials with different particle sizes reveals several interesting phenomena. First, the emerging low valence Mn<sup>2+</sup> specie on the surface is consistent with the oxygen release model, which takes place in the near-surface region, 34,43 leading to the continuous decrease of TM valence on the surface. Below, we will compare our analysis with three quantitative evaluations based on oxygen release of Li<sub>2</sub>MnO<sub>3</sub> sintered at 425°C, <sup>38</sup> 600°C, <sup>37</sup> and 800°C, <sup>43</sup> with 54%, 70%, and 70% of the initial charge capacity compensated by the released oxygen, respectively. All these gas release tests suggest oxygen release contributes to only part of the initial charge capacity.

Second, unlike the Mn-L spectra that could be quantitatively fitted by linearly combining reference spectra (Figures 2, 4, 5, S14, and S15), it is hard to quantify the number of carbonates based on only the O and C K-edge lineshapes. XAS is very sensitive to the  $\pi^*_{(C=O)}$  orbitals of carbonates through the distinct peaks and a clear peak could show up even with only a trace amount of carbonates. However, the qualitative contrast between the 400°C and 800°C samples on how sustainable the surface carbonate cycles, i.e., for only one cycle on 400°C (Figure \$10) but for 20 cycles on 800°C (Figure 5) samples, displays an intriguing consistency with the electrochemical profile associated with the high-voltage plateau: as shown in Figure S4, the dQ/dV curves of the 800°C electrodes display a weak but sustained oxidation reaction at the high voltage beyond the initial cycle. As a matter of fact, a weak kink at the high voltage could be seen directly on the voltage profile of the 800°C samples for at least the first 5 cycles. Although the amount of this high-voltage reaction is subtle after the initial charging, these experimental findings indicate that carbonate decomposition is associated with the charge plateau. We also note that previous experiments indeed found that Li<sub>2</sub>CO<sub>3</sub> decomposition takes place with a clear voltage plateau at 4.3-4.5 V with decomposition products of Li/Li<sub>2</sub>O, O<sub>2</sub>, and CO<sub>2</sub>.66-70

Third, we could now try to interpret the reaction mechanism of the initial charge plateau of Li<sub>2</sub>MnO<sub>3</sub> by combining the observations here and by checking the consistency with previous reports. Two distinct reactions take place within the Li<sub>2</sub>MnO<sub>3</sub> material itself and on the surface: (1) the delithiation of the Li<sub>2</sub>MnO<sub>3</sub> material itself. Because of the stable Mn<sup>4+</sup> bulk state during the initial charging (Figure 2) and the absence of lattice oxygen oxidation (Figure 1), the oxidation reaction associated with this delithiation leads to the oxygen release in the near-surface region, 34,43 as extensively studied in previous reports with partial contributions to the initial charge plateau. 37,38,43,44 This is also consistent with the clear signature of the Mn<sup>2+</sup> formation only on the particle surface (Figures 2, 4, and 5). Furthermore, the following discharge is dominated by Li-ion re-intercalation, leading to the Mn reduction in the material (Figures 2 and 3). (2) the surface carbonate decomposition. We emphasize again that this is not simply from the carbonate impurities from material synthesis that is often found in oxide electrodes, instead, this reaction is enabled by the carbonate formation on the pristine Li<sub>2</sub>MnO<sub>3</sub> particles before cycling (Figures 4 and 5).

For reaction (1), the delithiation in the low-temperature synthesized materials with small particle size, ~70 nm, and high capacity, ~290 mAh/g, displays the discharge capacity of 156 mAh/g from Li-ion re-intercalation (Figures 2 and 3). This value is 54% of





the initial charging capacity (290 mAh/q) but is complicated by the Coulomb efficiency that is counterbalanced by a trace amount of carbonate formation after the first charge, as discussed above. Yu et al. found that the oxygen release from Li<sub>2</sub>MnO<sub>3</sub> synthesized at roughly the same temperature (425°C) with the same particle size (70 nm) compensates 54% (190 mAh/g) of the initial charging capacity (350 mAh/g). 38 The exact match of the percentage (54%) here is likely just a coincidence. However, the consistency between the Li-ion re-intercalation during discharge and oxygen release data suggests that it is reasonable to expect  $\sim$ 50% of the initial charging capacity is from the  $\sim$ 70 nm material delithiation, which manifests itself as oxygen release. If we assume oxygen release takes place in the region of a fully delithiated phase, this means the oxygen release takes place within a layer of about 4.2 nm of the outer shell of a 70-nmsized Li<sub>2</sub>MnO<sub>3</sub> particle. This value is an effective thickness of the surface layer because the diffusion of Li-ions within the particle will blur the boundary, leading to a relatively thicker surface layer of oxygen release. Nonetheless, recent gas release and structural measurements show a highly delithiated layer of about 6 nm on Li<sub>2</sub>MnO<sub>3</sub> surface corresponding to the oxygen release region.<sup>43</sup>

For reaction (2),  $Li_2CO_3$  has a theoretical specific energy of 724 mAh/g with a 2.11 g/cm<sup>3</sup> material density, while the values are 459 mAh/g and 3.73 g/cm<sup>3</sup> for  $Li_2MnO_3$ . Based on these values, the decomposition of a layer of 3.8 nm of surface carbonate will compensate the other half of the initial charge capacity that is not from the oxygen release. Note again that this is an estimation based on a condensed  $Li_2CO_3$  layer. In reality, the thickness may be increased by other carbonate and/or organic components in the formation layer and by the typical amorphous structure of the surface interphase. However, in general, a thin layer of several nanometer thickness of carbonates seems to be enough to compensate for the part of the initial charging capacity besides the oxygen release.

For the high-temperature synthesized materials with 140 nm particle size and 82 mAh/g charging capacity, the discharge capacity (51 mAh/g) corresponding to the Li-ion re-intercalation is about 62% of the charging capacity. This is higher than that for 70 nm small particles described above but is again consistent with the higher value,  $\sim$ 70%, found in large particle materials on the oxygen release contribution. The contributions from oxygen release (51 mAh/g) and surface carbonates (31 mAh/g) require a  $\sim$ 2.7 nm thick layer of Li<sub>2</sub>MnO<sub>3</sub> on the surface for oxygen release and  $\sim$ 1.5 nm of carbonate formation.

A schematic of the rough estimation above is presented in Figure 6D. The estimation indicates an important difference between the 400°C (small) and 800°C (large) Li<sub>2</sub>MnO<sub>3</sub> particles: the smaller the particle size, the thicker a surface reaction region is involved. This seems to be counterintuitive but is understandable if one considers the low capacity of the large-sized particles, as well as the more efficient volume increase on the outer shell for larger particles. Therefore, the 800°C-synthesized large particle involves a thinner layer of surface reactions compared with the 400°C-synthesized small particle. As oxygen release triggers phase transformations from the pristine Li<sub>2</sub>MnO<sub>3</sub> phase toward more stable spinel phases, as found in many Li-rich compounds including Li<sub>2</sub>MnO<sub>3</sub>, <sup>44,49,51,52</sup> the pristine phase is thus sustained much better in the 800°C-synthesized larger particles, leading to a more sustained carbonate cycling. Therefore, consistent with the observations of a significant amount of carbonate formation on pristine material before cycling, the contrast between the 400°C and 800°C materials on the surface carbonate cycling indicates again that it is the pristine Li<sub>2</sub>MnO<sub>3</sub> phase that enables the surface carbonate activities.





#### Li<sub>2</sub>MnO<sub>3</sub> as an electrocatalyst for Li-CO<sub>2</sub> and Li-air batteries

As an intercalation type of electrode, it is almost impossible to maintain the pristine  $\text{Li}_2\text{MnO}_3$  phase due to the surface oxygen loss and phase transformations once the electrochemical charging starts. Additionally, the carbonate cycling in a standard LIB cell consumes the electrolyte, eliminating any practical application. Therefore, better utilization of the surface catalytic property of  $\text{Li}_2\text{MnO}_3$  is to employ the material in a catalytic system with a supply of reaction sources of carbonates, instead of using it as an intercalation type of electrode.

This hypothesis inspires us to test out a system based on  $CO_2$ /carbonate cycling with  $Li_2MnO_3$  electrocatalyst. We explored rechargeable  $Li-CO_2$ : $O_2$  (2:1) and  $Li-CO_2$  cells with  $Li_2MnO_3$  as the electrocatalyst (see technical details in Supplemental experimental procedures). Figures 7A and 7B display the electrochemical cycling of a  $Li-CO_2$ : $O_2$  (2:1) and a  $Li-CO_2$  cell with standard EC/DMC electrolyte, respectively. The  $800^{\circ}C$   $Li_2MnO_3$  is used as an electrocatalyst to facilitate the cycling of  $Li_2CO_3$ . Previous work has shown that  $Li-CO_2$ : $O_2$  could exhibit reversible behavior with carbonate cycling, however, the cyclability is very limited (10 cycles) and the voltage drop is significant even with an optimized electrolyte. Utilizing  $Li_2MnO_3$  catalyst clearly improves the cyclability here. Still, the  $Li-CO_2$  cells tend to fail after several cycles, due to the failure of electrolyte, although the cycling is partially reversible (Figures 7A and 7B). Replacing the electrolyte with  $LiCF_3SO_3$ /tetraethylene glycol dimethyl ether (TEGDME) (1:4) significantly improves the cycling stability. Figure 7C displays the  $30^{th}$  cycle of a  $Li-CO_2$ : $O_2$  (2:1) cell based on TEGDME electrolyte, with a capacity of 1,000 mAh  $g^{-1}$  (500 mAh  $g^{-1}$  for the full electrode).

O-K (Figures 7D and S17) and C-K (Figures 7E and S18) XAS confirm the disappear-ance/reappearance of the characteristic carbonate peaks at charged/discharged states. The SEM images show that a significant amount of surface layer is formed during the discharge process, covering up the pristine particles, but is largely decomposed with recovered morphology after charging (Figures 7F–7H). The reaction mechanism of the reversible cycling in Li-CO<sub>2</sub>/air batteries was proposed before as shown in Equation  $1^{68,69}$ :

$$2Li_2CO_3 + C \rightleftharpoons 4Li^+ + 3CO_2 + 4e^-$$
 (Equation 1)

Therefore, the voltage plateau around 4.2 V in the  $Li-CO_2$  cells stems from the carbonate decomposition, consistent but a bit lower than the 4.3–4.4V carbonate decomposition voltage with NiO and  $Co_3O_4$  in previous reports. <sup>66,67</sup> We also note that the discharge capacity here is also greatly improved over the systems based on those typical oxide electrocatalysts. <sup>66,67</sup> Additionally,  $Li_2MnO_3$  is of low cost compared with Ru and Au based systems, <sup>69</sup> indicating its superior potential on surface reactivity for catalytic reactions in Li-CO<sub>2</sub> and Li-air battery systems.

#### Commonality of the oxygen redox feature in Li-rich and conventional electrodes

The aforementioned holistic picture of the bulk and surface cycling mechanism of  $\text{Li}_2\text{MnO}_3$  suggests the dominating  $\text{Mn}^{3+/4+}$  redox reaction is responsible for the reversible part of the  $\text{Li}_2\text{MnO}_3$  cycling. This is in sharp contrast with the Li-rich electrodes, where a significant amount of reversible oxygen redox reaction could be observed through mRIXS. $^{2,9,12,16,29,33,48}$  For a direct comparison, we replotted in Figure S19 rough quantification results of the reversible redox reactions of  $\text{Li}_{1.17}\text{Ni}_{0.21}\text{Co}_{0.08}\text{Mn}_{0.54}\text{O}_2$  based on previous reports. $^{12,13}$  It is clear that the reversible oxygen redox reactions in Li-rich compounds are different from the  $\text{Li}_2\text{MnO}_3$  behaviors. We thus compare directly the oxidized oxygen mRIXS features between several representative systems.





Figure 8 presents the O-K mRIXS results of a series of fully charged electrodes of  $\text{Li}_{1.17}\text{Ni}_{0.21}\text{Co}_{0.08}\text{Mn}_{0.54}\text{O}_2 \text{ (Li-rich),}^{12} \text{LiNi}_{1/3}\text{Co}_{1/3}\text{Mn}_{1/3}\text{O}_2 \text{ (NCM111),}^{19} \text{LiCoO}_2,^{18}$ LiNiO<sub>2</sub>, <sup>17</sup> and Li<sub>2</sub>MnO<sub>3</sub>. Experimental details and results from pristine or discharged states of these electrodes are available in the previous reports. 12,17-19 Here, we concentrate on the fingerprinting mRIXS features of the oxidized oxygen found in these charged electrodes. Other than the broad features for all the compounds around 523-527 eV emission energy (horizontal axis), which stem from the strong TM-O hybridization, <sup>48</sup> all the charged electrodes, except for Li<sub>2</sub>MnO<sub>3</sub>, display the two fingerprinting features of the oxidized oxygen state: the feature around 531 excitation and 523.5 eV emission energies (red arrows) and the enhanced intensity close to the elastic line around the same excitation energy (light blue arrows).<sup>48</sup> Both features could be observed in typical oxidized oxygen references such as  $\text{Li}_2\text{O}_2$  and  $\text{O}_2.^{31,58}$  The former stands out from the broad hybridization feature, although it is relatively weak in LiNiO2, but the latter, although relatively weak, is also useful for particular analysis as they sit on a clean background far away from the hybridization feature. 16,48

Overall, the oxidized oxygen features found in the charged Li-rich, NCM111, Li-CoO<sub>2</sub>, and LiNiO<sub>2</sub> display a striking similarity, although with differences in both their spectral intensities and energy positions for a small amount (see the horizontal and vertical while lines as guides to eyes). We note here that these are all 3d TMO compounds and some TM systems with oxygen redox reactions could display a more significant difference in the energy values in spectroscopy. In sharp contrast, such oxidized oxygen features are absent in Li<sub>2</sub>MnO<sub>3</sub>, as discussed in this work. Figure 8F further plotted the RIXS lineshape comparison of all the samples collected at 531 eV excitation energy, where the contrast between Li-rich and Li<sub>2</sub>MnO<sub>3</sub>, as well as the similarity between Li-rich and the non-Li-rich conventional materials, could be clearly seen. The comparison indicates that the oxygen redox reaction in Li-rich is of the same nature as those that emerge in non-Li-rich conventional compounds; however, the Li-rich parent compound, Li<sub>2</sub>MnO<sub>3</sub> cannot maintain any lattice oxidized oxygen state for reversible oxygen redox reactions.

During the review process of this work, the energy-loss features close to the elastic line has been resolved and used as evidence for a new oxygen redox model based on reversible formation and reduction of "trapped O<sub>2</sub> molecules<sup>21,59</sup>," and we were asked to discuss the possible association between our findings here and this new model. Although it seems there could be a possibility that all formed O<sub>2</sub> molecules escape from the Li<sub>2</sub>MnO<sub>3</sub> material, leading to the absence of mRIXS features on oxidized oxygen, our experimental observations indicate this is not likely the case. Our results show that different particle sizes of 70 and 140 nm have no effect on the absence of oxidized oxygen feature in mRIXS (Figure 1); however, they display a 3 times difference in the initial charging capacity (Figure S5). If the formation of O<sub>2</sub> is the major reaction mechanism during charging with a complete release, the specific capacity should be more or less the same, which directly contradicts the 3 times difference in experimental results. Additionally, for Li-rich electrodes that do display the mRIXS oxygen redox features, the reversible behavior of the appearance and disappearance of the mRIXS features has been found over 500 cycles. 12 Fairly stable oxygen redox reactions were also found in Na-ion systems for a hundred cycles with strong signatures of such energy-loss features. 13 Extended cycles of Li-rich electrode display only slow voltage fade instead of the voltage plateau and strong hysteresis during the initial cycle, which indicates that if the trapped O<sub>2</sub> model is responsible to the hysteresis and plateau during the initial cycle, <sup>59</sup> the practically meaningful reversible oxygen redox reaction in Li-rich compounds should be of a





different origin. Therefore, it remains an open question on whether the resolved phonon features, which seems to be close to  $O_2$  vibronic modes could conclude the nature of the oxidized oxygen mechanism as trapped  $O_2$  molecules, especially considering the same feature is sustained after hundreds of cycles in battery materials. Additionally, other experiments that detect the vibronic modes associated with the oxidized oxygen states in Li-rich materials, e.g., Raman spectroscopy, found the vibronic frequency of the solid-state peroxo-specie,  $^{72}$  instead of the vibronic mode of  $O_2$  molecules. Sitting at the center of these puzzles is the clarification of the fundamental picture of oxygen redox reactions and the fundamental origin of these key RIXS features.

#### **Conclusions and perspectives**

In summary, this work clarifies the bulk and surface chemistry involved in the electrochemical activities of the  $\rm Li_2MnO_3$  material. The clarifications based on systematic and comparative studies of a sample with different synthesis conditions lead to two groups of technical findings and two major conclusions.

For the bulk chemistry, our quantitative analysis of the Mn redox reactions through Mn-L mRIXS-iPFY, combined with the searching of lattice oxygen redox through O-K mRIXS, concludes the Li<sub>2</sub>MnO<sub>3</sub> bulk cycling mechanism: the oxygen activities during the initial charging of Li<sub>2</sub>MnO<sub>3</sub> contain no reversible lattice oxygen redox at any voltage. The following discharge capacity is from a complete crossover to Mn<sup>3+/4+</sup> redox reactions, which could be quantified and agrees with the electrochemical capacity. The  $2^{\rm nd}$  cycle charging is a majority Mn<sup>3+/4+</sup> oxidation process, but with a small amount of non-Mn reactions, followed again by a pure Mn<sup>3+/4+</sup> reduction during the  $2^{\rm nd}$  discharge. Our results rule out both the reversible oxygen redox scenario and the Mn<sup>4+/7+</sup> models. Additionally, analysis of Li<sub>2</sub>MnO<sub>3</sub> materials with different particle sizes, which display a 3-times contrast on capacities, but no difference on the absence of the oxidized oxygen signature, disagrees with the recently proposed trapped O<sub>2</sub> model and also indicates the important role of surface reactions.

For the surface chemistry, we performed a detailed evaluation of the surface chemistry of Li<sub>2</sub>MnO<sub>3</sub> based on surface-sensitive spectroscopy with quantitative analysis. We found an intriguing carbonate formation and decomposition over extended cycles on the surface of relatively large (better crystallized) Li<sub>2</sub>MnO<sub>3</sub> particles. This is accompanied by evidence of a highly reactive Li<sub>2</sub>MnO<sub>3</sub> surface and continuously accumulated Mn<sup>2+</sup> species on the surface. We note that, although the existence of Li<sub>2</sub>CO<sub>3</sub> on the surface of Li-rich compounds has been observed before,  $^{38,67,70,73}$  it was typically considered to be the results of the oxygen evolution from Li<sub>2</sub>MnO<sub>3</sub> after electrochemical cycling. Here, we show that the high reactivity is an intrinsic surface property of pristine Li<sub>2</sub>MnO<sub>3</sub> before any electrochemical cycling. The surface carbonates formed on the pristine Li<sub>2</sub>MnO<sub>3</sub> material before cycling get decomposed during the initial charging plateau. The combination of the oxygen release and surface carbonate decomposition, both in the near-surface region, is responsible for the high-voltage charging plateau of Li<sub>2</sub>MnO<sub>3</sub>.

The findings of the highly active catalytic properties of the pristine  $Li_2MnO_3$  surface inspires the concept of utilizing  $Li_2MnO_3$  not as an intercalation material but as an electrocatalyst to improve the carbonate cycling in  $Li-CO_2$  and Li-air battery systems. We, therefore, tested three different systems with  $Li_2MnO_3$  acting as an electrocatalyst, which demonstrates that  $Li_2MnO_3$  is indeed an effective catalytic material for the carbonate formation and decomposition. This opens up a broad field on utilizing alkali-rich oxide materials as catalysts for not only Li-air, Li- $CO_2$ , and fuel cell





applications but also other emerging battery systems, such as  $Na^+$ ,  $Mg^{2+}$ , and  $Al^{3+}$  batteries, in which greenhouse gas could be captured and utilized to achieve reversible energy storage.

The absence of lattice oxygen redox chemistry in Li<sub>2</sub>MnO<sub>3</sub> motivates further investigations on the origin of the reversible oxygen redox reactions found in Li-rich materials. Comparisons between the Li-rich, Li<sub>2</sub>MnO<sub>3</sub>, and conventional materials such as NCM111, LiCoO<sub>2</sub>, and LiNiO<sub>2</sub>, reveals that the reversible oxygen redox features found in Li-rich (xLi<sub>2</sub>MnO<sub>3</sub>·(1-x)LiMO<sub>2</sub>) resemble those in conventional compounds, whereas Li<sub>2</sub>MnO<sub>3</sub> exhibit no signature of reversible oxygen redox. These similarities and contrasts, strongly suggest that the reversible oxygen redox reaction is a property of TM oxide cathode at high voltages regardless of Li-rich or not. On the contrary, Li<sub>2</sub>MnO<sub>3</sub>, as the extreme case of the Li-rich configuration, displays only irreversible oxygen release with no lattice oxygen redox involved. However, previous reports show that the oxygen redox reaction in Li-rich system could be sustained over hundreds of cycles, while most oxygen redox in conventional materials decay quickly upon cycling. Therefore, the Li-rich configuration should be considered as a modulator that could affect the oxygen redox behavior, by either improving its cyclability or over-promoting the oxygen oxidation into the irreversible oxygen release. Nonetheless, the spectroscopic comparison implies that the driving force and the nature of the oxygen redox reaction are the same in both Li-rich and non-Li-rich conventional compounds.

It is important to note that the conclusion on the common nature of the oxygen redox in oxide cathodes here is by no means to despise the many seminal works on the oxygen activities in Li-rich compounds, which directly inspired this work. However, properties of Li-rich systems, e.g., cation migrations, structural phase transitions, and local chemical bond configurations are no longer considered the fundamental driving force of oxygen redox reaction here but could be coupled with and modify the oxygen redox activities. These modification effects from Li-rich configuration have indeed been found to change the oxygen redox reversibility, voltages, kinetics, and stability. These effects could sometimes be beneficial, e.g., the improved reversibility of oxygen redox in Li-rich compounds over conventional materials, but other times be detrimental, e.g., over-promoting oxygen oxidation to irreversible oxygen release as in the case of Li<sub>2</sub>MnO<sub>3</sub>. As a matter of fact, examples of such modulation effects could be seen in many pieces of literature. For example, a recent study of a "rejuvenation" effect in Li-rich materials found that the change of local ordering associated with oxygen redox leads to better kinetics upon the cycling of Li-rich materials.<sup>74</sup> Other works indicate that the irreversible oxygen activities in Li<sub>2</sub>MnO<sub>3</sub> could be enabled through stoichiometry, structural variations, surface coatings, and elemental doping. A direct demonstration is the emergence of oxygen redox reaction in the acid-treated Li<sub>2</sub>MnO<sub>3</sub> system. <sup>75</sup> Understanding these modification mechanisms from the Li-rich configuration, instead of taking it as the fundamental trigger of oxygen redox, is vital for understanding and improving oxygen redox-based cathodes.

Fundamentally, emphasizing the common nature of the lattice oxygen redox in TM oxide cathodes should be differentiated from the universally existing TM–O hybridization in TM oxides. As we defined at the beginning of this work, changes in oxygen electron density through covalency or hybridization should be differentiated from the oxygen redox concept here. The common behavior of lattice oxygen redox in both conventional and Li-rich electrodes also implies that the true fundamental driving force of oxygen redox activities is beyond models built on Li-rich





configurations. More importantly, this commonality naturally points the fundamental origin of oxygen redox to the primitive TMO system with a driving force applicable for all, or almost all, TMOs under highly oxidized states, instead of a specific oxygen orbital configuration or a particular material configuration. A direct theoretical calculation of the critical mRIXS features in TMO without arbitrary parameters remains the key for understanding this fundamental driving force of lattice oxygen redox reactions, which remains a grand challenge to the fields of both fundamental physics and material sciences.

Finally, it is worth noting that some of the non-alkali-rich conventional Na-ion compounds not only exhibit strong oxygen redox activities but also display superior properties of facile kinetics of the oxygen redox reactions, 20,21 which is notoriously sluggish in Li-rich systems and has been formidable to be improved.<sup>7</sup> Therefore, it seems some conventional materials under certain circumstances have their own beneficial effects on the oxygen redox behaviors. Of course, practical developments of oxygen redox-based electrodes also require other significant efforts, e.g., highvoltage electrolyte, than just the cathode material itself. Our comparison also indicates that the oxygen redox behaviors in conventional materials vary among different TM systems, e.g., it seems to be relatively suppressed in the Ni system that is of interest for the Ni-rich material explorations. Comparative studies between the many conventional systems with different compositions and stoichiometry will likely open opportunities for rich sciences and great potentials for high-voltage battery operations. While scientists are pursuing the ultimate clarifications of the oxygen redox mechanism, the quickly evolving machine learning algorithms could be practically useful to reveal the underlying composition-chemistry-performance correlations related with the complex oxygen activities in the vast field of conventional cathode materials, which have not been explored as much as those for Li-rich compounds on its high-voltage and oxygen behaviors.

#### **EXPERIMENTAL PROCEDURES**

#### Resource availability

#### Lead contact

Further information and requests should be directed to and will be fulfilled by the Lead Contact, Wanli Yang (wlyang@lbl.gov).

#### Materials availability

The materials in this study are standard and have been reported multiple times by many groups. Full details of all experiments and materials are provided in Supplemental information.

#### Data and code availability

This study does not generate any code.

#### SUPPLEMENTAL INFORMATION

Supplemental information can be found online at https://doi.org/10.1016/j.joule. 2021.02.004.

#### **ACKNOWLEDGMENTS**

Spectroscopic experiments were performed at the BL8.0.1.1 (iRIXS) (all except Li-K) and BL4.0.3 (MERIXS) (for Li-K) endstations at the Advanced Light Source (ALS), a USA DOE Office of Science User Facility at Lawrence Berkeley National Laboratory (LBNL). W.Y. thanks DOE Data, Artificial Intelligence, and Machine Learning at





DOE Scientific User Facilities project for their support, Z.Z. and J.W. thank the ALS fellowship program for its support. All LBNL efforts are under DOE contract no. DE-AC02-05CH11231. Z.Z. and F.P. thank National Key R&D Program of China (2016YFB0700600). The work at IOP CAS was supported by National Key R&D Program of China (grants no. 2016YFB0100100), Beijing Municipal Science and Technology Commission (grants no. D181100004518003), and the National Natural Science Foundation of China (51822211, U1964205, Y5JC011E21). Works at Stanford are supported by the U.S. DOE, Office of Basic Energy Sciences, Division of Materials Sciences and Engineering under contract no. DE-AC0276SF00515.

#### **AUTHOR CONTRIBUTIONS**

W.Y. and H.L. conceived the project. W.Y., H.L., T.P.D., and F.P. coordinated the collaborative efforts in materials, characterizations, and interpretations with all authors involved. Z.Z. performed RIXS spectroscopic experiments. R.Q. performed XAS experiments. K.D. and R.W. synthesized the material and performed electrochemical tests. Y.L. performed the Li-CO<sub>2</sub> and Li-air battery tests. W.Y., Z.Z., K.D., R.Q., and R.W. wrote the paper with discussions and inputs from all authors.

#### **DECLARATION OF INTERESTS**

The authors declare no competing interests.

Received: June 8, 2020 Revised: November 24, 2020 Accepted: February 10, 2021 Published: March 4, 2021

#### REFERENCES

- 1. Li, W., Song, B., and Manthiram, A. (2017). High-voltage positive electrode materials for lithium-ion batteries. Chem. Soc. Rev. 46, 3006-3059
- 2. Li, M., Liu, T., Bi, X., Chen, Z., Amine, K., Zhong, C., and Lu, J. (2020). Cationic and anionic redox in lithium-ion based batteries. Chem. Soc. Rev. 49, 1688-1705.
- 3. Goodenough, J.B., and Kim, Y. (2010). Challenges for rechargeable Li batteries †. Chem. Mater. 22, 587-603.
- 4. Ellis, B.L., Lee, K.T., and Nazar, L.F. (2010). Positive electrode materials for Li-Ion and Libatteries †. Chem. Mater. 22, 691-714.
- 5. Grimaud, A., Hong, W.T., Shao-Horn, Y., and Tarascon, J.M. (2016). Anionic redox processes for electrochemical devices. Nat. Mater. 15,
- 6. Wu, J., Zhuo, Z., Rong, X., Dai, K., Lebens-Higgins, Z., Sallis, S., Pan, F., Piper, L.F.J., Liu, G., Chuang, Y.-D., et al. (2020). Dissociate lattice oxygen redox reactions from capacity and voltage drops of battery electrodes. Sci. Adv. 6, eaaw3871.
- 7. Assat, G., and Tarascon, J.-M. (2018). Fundamental understanding and practical challenges of anionic redox activity in Li-ion batteries. Nat. Energy 3, 373–386.
- 8. Seo, D.H., Lee, J., Urban, A., Malik, R., Kang, S., and Ceder, G. (2016). The structural and chemical origin of the oxygen redox activity in

- layered and cation-disordered Li-excess cathode materials. Nat. Chem. 8, 692-697.
- 9. Luo, K., Roberts, M.R., Hao, R., Guerrini, N., Pickup, D.M., Liu, Y.-S., Edström, K., Guo, J., Chadwick, A.V., Duda, L.C., et al. (2016). Charge-compensation in 3d-transition-metaloxide intercalation cathodes through the generation of localized electron holes on oxygen. Nat. Chem. 8, 684–691.
- 10. McCalla, E., Abakumov, A.M., Saubanère, M., Foix, D., Berg, E.J., Rousse, G., Doublet, M.-L., Gonbeau, D., Novák, P., Van Tendeloo, G., et al. (2015). Visualization of O-O peroxo-like dimers in high-capacity layered oxides for Liion batteries. Science 350, 1516-1521.
- 11. Thackeray, M.M., Kang, S.-H., Johnson, C.S. Vaughey, J.T., Benedek, R., and Hackney, S.A. (2007). Li2MnO3-stabilized LiMO2 (M = Mn, Ni, Co) electrodes for lithium-ion batteries. J. Mater. Chem. 17, 3112-3125.
- 12. Gent, W.E., Lim, K., Liang, Y., Li, Q., Barnes, T., Ahn, S.-J., Stone, K.H., McIntire, M., Hong, J., Song, J.H., et al. (2017). Coupling between oxygen redox and cation migration explains unusual electrochemistry in lithium-rich layered oxides. Nat. Commun. 8, 2091.
- Dai, K., Wu, J., Zhuo, Z., Li, Q., Sallis, S., Mao, J., Ai, G., Sun, C., Li, Z., Gent, W.E., et al. (2018). High reversibility of lattice oxygen redox quantified by direct bulk probes of both anionic and cationic redox reactions. Joule 3, 518-541.

- 14. Lee, J., Kitchaev, D.A., Kwon, D.H., Lee, C.W., Papp, J.K., Liu, Y.S., Lun, Z.Y., Clément, R.J., Shi, T., McCloskey, B.D., et al. (2018). Reversible Mn2+/Mn4+ double redox in lithium-excess cathode materials. Nature 556, 185-190.
- 15. Clément, R.J., Lun, Z., and Ceder, G. (2020). Cation-disordered rocksalt transition metal oxides and oxyfluorides for high energy lithium-ion cathodes. Energy Environ. Sci. 13, 345-373.
- 16. Lebens-Higgins, Z.W., Faenza, N.V., Radin, M.D., Liu, H., Sallis, S., Rana, J., Vinckeviciute, J., Reeves, P.J., Zuba, M.J., Badway, F., et al. (2019). Revisiting the charge compensation mechanisms in LiNi 0.8 Co 0.2-y Al y O 2 systems. Mater. Horiz. 6, 2112-2123.
- 17. Li, N., Sallis, S., Papp, J.K., Wei, J., McCloskey, B.D., Yang, W., and Tong, W. (2019). Unraveling the cationic and anionic redox reactions in a conventional layered oxide cathode. ACS Energy Lett. 4, 2836-2842.
- 18. Zhang, J.-N., Li, Q., Ouyang, C., Yu, X., Ge, M., Huang, X., Hu, E., Ma, C., Li, S., Xiao, R., et al. (2019). Trace doping of multiple elements enables stable battery cycling of LiCoO2 at 4.6 V. Nat. Energy 4, 594–603.
- 19. Lee, G.-H., Wu, J., Kim, D., Cho, K., Cho, M., Yang, W., and Kang, Y.-M. (2020). Reversible anionic redox activities in conventional LiNi1/ 3Co1/3Mn1/3O2 cathodes. Angew. Chem. Int. Ed. Engl. 132, 8759-8766.





- Dai, K., Mao, J., Zhuo, Z., Feng, Y., Mao, W., Ai, G., Pan, F., Chuang, Y.-d., Liu, G., and Yang, W. (2020). Negligible voltage hysteresis with strong anionic redox in conventional battery electrode. Nano Energy 74, 104831.
- House, R.A., Maitra, U., Pérez-Osorio, M.A., Lozano, J.G., Jin, L., Somerville, J.W., Duda, L.C., Nag, A., Walters, A., Zhou, K.-J., et al. (2020). Superstructure control of first-cycle voltage hysteresis in oxygen-redox cathodes. Nature 577, 502–508.
- Maitra, U., House, R.A., Somerville, J.W., Tapia-Ruiz, N., Lozano, J.G., Guerrini, N., Hao, R., Luo, K., Jin, L., Pérez-Osorio, M.A., et al. (2018). Oxygen redox chemistry without excess alkalimetal ions in Na2/3[Mg0.28Mn0.72]O2. Nat. Chem. 10, 288–295.
- Chen, H., and Islam, M.S. (2016). Lithium extraction mechanism in Li-Rich Li2MnO3 involving oxygen hole formation and dimerization. Chem. Mater. 28, 6656–6663.
- Xie, Y., Saubanère, M., and Doublet, M.-L. (2017). Requirements for reversible extracapacity in Li-rich layered oxides for Li-ion batteries. Energy Environ. Sci. 10, 266–274.
- Saubanère, M., McCalla, E., Tarascon, J.-M., and Doublet, M.-L. (2016). The intriguing question of anionic redox in high-energy density cathodes for Li-ion batteries. Energy Environ. Sci. 9, 984–991.
- Oishi, M., Yamanaka, K., Watanabe, I., Shimoda, K., Matsunaga, T., Arai, H., Ukyo, Y., Uchimoto, Y., Ogumi, Z., and Ohta, T. (2016). Direct observation of reversible oxygen anion redox reaction in Li-rich manganese oxide, Li2MnO3, studied by soft X-ray absorption spectroscopy. J. Mater. Chem. A 4, 9293–9302.
- Han, S.J., Xia, Y.G., Wei, Z., Qiu, B., Pan, L.C., Gu, Q.W., Liu, Z.P., and Guo, Z.Y. (2015). A comparative study on the oxidation state of lattice oxygen among Li1.14Ni0.136Co0.136Mn0.544O2, Li2MnO3, LiNi0.5Co0.2Mn0.3O2 and LiCoO2 for the initial charge–discharge. J. Mater. Chem. A 3, 11930–11939.
- 28. Massel, F., Hikima, K., Rensmo, H., Suzuki, K., Hirayama, M., Xu, C., Younesi, R., Liu, Y.-S., Guo, J., Kanno, R., et al. (2019). Excess lithium in transition metal layers of epitaxially grown thin film cathodes of Li2MnO3 leads to rapid loss of covalency during first battery cycle. J. Phys. Chem. C 123, 28519–28526.
- Xu, J., Sun, M., Qiao, R., Renfrew, S.E., Ma, L., Wu, T., Hwang, S., Nordlund, D., Su, D., Amine, K., et al. (2018). Elucidating anionic oxygen activity in lithium-rich layered oxides. Nat. Commun. 9, 947.
- 30. Ji, H., Wu, J., Cai, Z., Liu, J., Kwon, D.-H., Kim, H., Urban, A., Papp, J.K., Foley, E., Tian, Y., et al. (2020). Ultrahigh power and energy density in partially ordered lithium-ion cathode materials. Nat. Energy 5, 213–221.
- Zhuo, Z., Liu, Y.S., Guo, J., Chuang, Y.D., Pan, F., and Yang, W. (2020). Full energy Range resonant inelastic X-ray scattering of O2 and CO2: direct comparison with oxygen redox state in batteries. J. Phys. Chem. Lett. 11, 2618– 2623.
- 32. Roychoudhury, S., Qiao, R., Zhuo, Z., Li, Q., Lyu, Y., Kim, J.-H., Liu, J., Lee, E., Polzin, B.J., Guo,

- J., et al. (2020). Deciphering the oxygen absorption pre-edge: a caveat on its application for probing oxygen redox reactions in batteries. Energy Environ. Mater. https://doi.org/10.1002/eem2.12119.
- 33. Yang, W. (2018). Oxygen release and oxygen redox. Nat. Energy 3, 619–620.
- 34. House, R.A., Maitra, U., Jin, L., Lozano, J.G., Somerville, J.W., Rees, N.H., Naylor, A.J., Duda, L.C., Massel, F., Chadwick, A.V., et al. (2019). What triggers oxygen loss in oxygen redox cathode materials? Chem. Mater. 31, 3293–3300.
- Lu, Z., and Dahn, J.R. (2002). Understanding the anomalous capacity of Li/Li[NixLi(1/3-2x/3) Mn(2/3-x/3)]O2 cells using in situ x-ray diffraction and electrochemical studies.
   J. Electrochem. Soc. 149, A815-A822.
- Radin, M.D., Vinckeviciute, J., Seshadri, R., and Van der Ven, A. (2019). Manganese oxidation as the origin of the anomalous capacity of Mncontaining Li-excess cathode materials. Nat. Energy 4, 639–646.
- Rana, J., Papp, J.K., Lebens-Higgins, Z., Zuba, M., Kaufman, L.A., Goel, A., Schmuch, R., Winter, M., Whittingham, M.S., Yang, W., et al. (2020). Quantifying the capacity contributions during activation of Li2MnO3. ACS Energy Lett. 5, 634–641.
- Yu, D.Y.W., Yanagida, K., Kato, Y., and Nakamura, H. (2009). Electrochemical activities in Li2MnO3. J. Electrochem. Soc. 156, A417.
- Yang, W., and Devereaux, T.P. (2018). Anionic and cationic redox and interfaces in batteries: advances from soft X-ray absorption spectroscopy to resonant inelastic scattering. J. Power Sources 389, 188–197.
- Kalyani, P., Chitra, S., Mohan, T., and Gopukumar, S. (1999). Lithium metal rechargeable cells using Li2MnO3 as the positive electrode. J. Power Sources 80, 103–106.
- Robertson, A.D., and Bruce, P.G. (2002). The origin of electrochemical activity in Li2MnO3. Chem. Commun. 2790–2791.
- 42. Lebens-Higgins, Z.W., Chung, H., Zuba, M.J., Rana, J., Li, Y., Faenza, N.V., Pereira, N., McCloskey, B.D., Rodolakis, F., Yang, W., et al. (2020). How bulk sensitive is hard X-ray photoelectron spectroscopy: accounting for the cathode–electrolyte interface when addressing oxygen redox. J. Phys. Chem. Lett. 11, 2106–2112.
- Guerrini, N., Jin, L., Lozano, J.G., Luo, K., Sobkowiak, A., Tsuruta, K., Massel, F., Duda, L.-C., Roberts, M.R., and Bruce, P.G. (2020). Charging mechanism of Li2MnO3. Chem. Mater. 32, 3733–3740.
- Strehle, B., Kleiner, K., Jung, R., Chesneau, F., Mendez, M., Gasteiger, H.A., and Piana, M. (2017). The role of oxygen release from Li- and Mn-rich layered oxides during the first cycles investigated by on-line electrochemical mass spectrometry. J. Electrochem. Soc. 164, A400– A406.
- 45. Zuba, Mateusz Jan, Grenier, Antonin, Lebens-Higgins, Zachary, Paez Fajardo, Galo J., Li, Yixuan, Ha, Yang, et al. (2021). Whither Mn Oxidation in Mn-Rich Alkali-Excess Cathodes?

- ACS Energy Lett. 6, 1055–1064, https://doi.org/10.1021/acsenergylett.0c02418.
- 46. Gent, W.E., Abate, I.I., Yang, W., Nazar, L.F., and Chueh, W.C. (2020). Design rules for high-valent redox in intercalation electrodes. Joule 4, 1369–1397.
- Li, Q., Lebens-Higgins, Z.W., Li, Y., Meng, Y.S., Chuang, Y.D., Piper, L.F.J., Liu, Z., and Yang, W. (2021). Could irradiation introduce oxidized oxygen signals in resonant inelastic X-ray scattering of battery electrodes? J. Phys. Chem. Lett. 12, 1138–1143.
- 48. Wu, J., Li, Q., Sallis, S., Zhuo, Z., Gent, W.E., Chueh, W.C., Yan, S., Chuang, Y.-d., and Yang, W. (2019). Fingerprint oxygen redox reactions in batteries through high-efficiency mapping of resonant inelastic X-ray scattering. Condens. Matter 4 5
- Wang, R., He, X., He, L., Wang, F., Xiao, R., Gu, L., Li, H., and Chen, L. (2013). Atomic structure of Li2MnO3 after partial delithiation and re-Lithiation. Adv. Energy Mater. 3, 1358–1367.
- Qiao, R., Dai, K., Mao, J., Weng, T.-C., Sokaras, D., Nordlund, D., Song, X., Battaglia, V.S., Hussain, Z., Liu, G., and Yang, W. (2015). Revealing and suppressing surface Mn(II) formation of Na0.44MnO2 electrodes for Naion batteries. Nano Energy 16, 186–195.
- Yu, D.Y.W., and Yanagida, K. (2011). Structural analysis of Li2MnO3 and related Li-Mn-O materials. J. Electrochem. Soc. 158, A1015.
- Gu, M., Belharouak, I., Zheng, J., Wu, H., Xiao, J., Genc, A., Amine, K., Thevuthasan, S., Baer, D.R., Zhang, J.-G., et al. (2013). Formation of the spinel phase in the layered composite cathode used in Li-ion batteries. ACS Nano 7, 760–767
- Yang, Y., Su, H., Wu, T., Jiang, Y., Liu, D., Yan, P., Tian, H., and Yu, H. (2019). Atomic pair distribution function research on Li2MnO3 electrode structure evolution. Sci. Bull. 64, 553-561.
- Francis Amalraj, S., Markovsky, B., Sharon, D., Talianker, M., Zinigrad, E., Persky, R., Haik, O., Grinblat, J., Lampert, J., Schulz-Dobrick, M., et al. (2012). Study of the electrochemical behavior of the "inactive" Li2MnO3. Electrochim. Acta 78, 32–39.
- Boulineau, A., Croguennec, L., Delmas, C., and Weill, F. (2009). Reinvestigation of Li2MnO3 structure: electron diffraction and high resolution TEM. Chem. Mater. 21, 4216–4222.
- Amalraj, S.F., Sharon, D., Talianker, M., Julien, C.M., Burlaka, L., Lavi, R., Zhecheva, E., Markovsky, B., Zinigrad, E., Kovacheva, D., et al. (2013). Study of the nanosized Li2MnO3: electrochemical behavior, structure, magnetic properties, and vibrational modes. Electrochim. Acta 97, 259–270.
- Rana, J., Stan, M., Kloepsch, R., Li, J., Schumacher, G., Welter, E., Zizak, I., Banhart, J., and Winter, M. (2014). Structural changes in Li2MnO3 cathode material for Li-ion batteries. Adv. Energy Mater. 4, 1300998.
- 58. Zhuo, Z., Pemmaraju, C.D., Vinson, J., Jia, C., Moritz, B., Lee, I., Sallies, S., Li, Q., Wu, J., Dai, K., et al. (2018). Spectroscopic signature of oxidized oxygen states in peroxides. J. Phys. Chem. Lett. 9, 6378–6384.

## **Joule** Article



- 59. House, R.A., Rees, G.J., Pérez-Osorio, M.A., Marie, J.-J., Boivin, E., Robertson, A.W., Nag, A., Garcia-Fernandez, M., Zhou, K.-J., and Bruce, P.G. (2020). First-cycle voltage hysteresis in Li-rich 3d cathodes associated with molecular O2 trapped in the bulk. Nat. Energy 5. 777-785.
- 60. Hu, E., Yu, X., Lin, R., Bi, X., Lu, J., Bak, S., Nam, K.-W., Xin, H.L., Jaye, C., Fischer, D.A., et al. (2018). Evolution of redox couples in Li- and Mn-rich cathode materials and mitigation of voltage fade by reducing oxygen release. Nat. Energy 3, 690–698.
- 61. Manceau, A., Marcus, M.A., and Grangeon, S. (2012). Determination of Mn valence states in mixed-valent manganates by XANES spectroscopy. Am. Mineral. 97, 816–827.
- 62. Li, Q., Qiao, R., Wray, L.A., Chen, J., Zhuo, Z., Chen, Y., Yan, S., Pan, F., Hussain, Z., and Yang, W. (2016). Quantitative probe of the transition metal redox in battery electrodes through soft x-ray absorption spectroscopy. J. Phys. D Appl. Phys. 49, 413003.
- 63. Wandt, J., Freiberg, A.T.S., Ogrodnik, A., and Gasteiger, H.A. (2018). Singlet oxygen evolution from layered transition metal oxide cathode materials and its implications for lithium-ion batteries. Mater. Today 21, 825-833.
- 64. Ohzuku, T., Nagayama, M., Tsuji, K., and Ariyoshi, K. (2011). High-capacity lithium

- insertion materials of lithium nickel manganese oxides for advanced lithium-ion batteries: toward rechargeable capacity more than 300 mA h g-1. J. Mater. Chem. 21, 10179.
- 65. Johnson, C.S., Li, N., Lefief, C., and Thackeray, M.M. (2007). Anomalous capacity and cycling stability of xLi2MnO3·(1-x)LiMO2 electrodes (M=Mn, Ni, Co) in lithium batteries at 50°C. Electrochem. Commun. 9, 787-795.
- 66. Wang, R., Yu, X., Bai, J., Li, H., Huang, X., Chen, L., and Yang, X. (2012). Electrochemical decomposition of Li2CO3 in NiO-Li2CO3 nanocomposite thin film and powder electrodes. J. Power Sources 218, 113-118.
- 67. Yabuuchi, N., Yoshii, K., Myung, S.T., Nakai, I., and Komaba, S. (2011). Detailed studies of a high-capacity electrode material for rechargeable batteries, Li2MnO3–LiCo1/ 3Ni1/3Mn1/3O2. J. Am. Chem. Soc. 133, 4404-4419
- 68. Liu, Y., Wang, R., Lyu, Y., Li, H., and Chen, L. (2014). Rechargeable Li/CO2–O2 (2: 1) battery and Li/CO2 battery. Energy Environ. Sci. 7, 677.
- 69. Qiao, Y., Yi, J., Wu, S., Liu, Y., Yang, S., He, P., and Zhou, H. (2017). Li-CO 2 electrochemistry: a new strategy for CO 2 fixation and energy storage. Joule 1, 359–370.
- 70. Hong, J., Lim, H.-D., Lee, M., Kim, S.-W., Kim, H., Oh, S.-T., Chung, G.-C., and Kang, K. (2012).

- Critical role of oxygen evolved from layered Liexcess metal oxides in lithium rechargeable batteries. Chem. Mater. 24, 2692-2697.
- 71. Bruce, P.G., Freunberger, S.A., Hardwick, L.J., and Tarascon, J.M. (2011). Li-O2 and Li-S batteries with high energy storage. Nat. Mater. 11, 19-29.
- 72. Li, X., Qiao, Y., Guo, S., Xu, Z., Zhu, H., Zhang, X., Yuan, Y., He, P., Ishida, M., and Zhou, H. (2018). Direct visualization of the reversible O2-/O- redox process in Li-Rich cathode materials. Adv. Mater. 30, e1705197.
- 73. Oishi, M., Yogi, C., Watanabe, I., Ohta, T., Orikasa, Y., Uchimoto, Y., and Ogumi, Z. (2015). Direct observation of reversible charge compensation by oxygen ion in Li-rich manganese layered oxide positive electrode material, Li1.16Ni0.15 Co0.19 Mn0.50 O2. J. Power Sources 276, 89-94.
- 74. Lee, J., Yu, D., Zhu, Z., Yao, X., Wang, C., Dong, Y., Malik, R., and Li, J. (2020). Kinetic rejuvenation of Li-rich Li-lon battery cathodes upon oxygen redox. ACS Appl. Energy Mater. 3, 7931–7943.
- 75. Wu, J., Zhang, X., Zheng, S., Liu, H., Wu, J., Fu, R., Li, Y., Xiang, Y., Liu, R., Zuo, W., et al. (2020). Tuning oxygen redox reaction through the inductive effect with proton insertion in Li-rich oxides. ACS Appl. Mater. Interfaces 12, 7277-7284